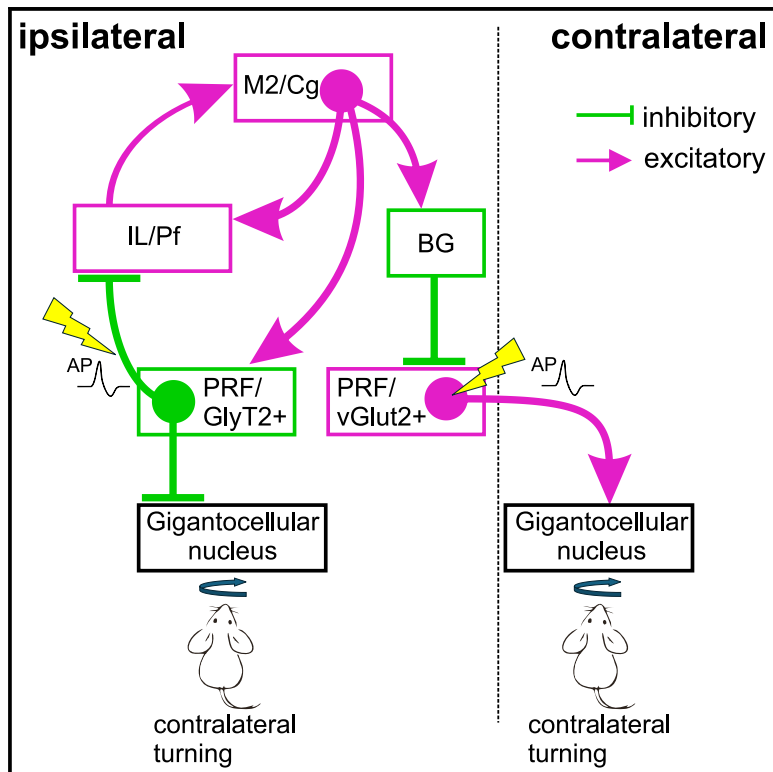


A cortico-subcortical loop for motor control via the pontine reticular formation

Graphical abstract



Authors

Emília Bősz, Viktor M. Plattner,
László Biró, Kata Kóta, Marco A. Diana,
László Acsády

Correspondence

acsady@koki.hu

In brief

Bősz et al. reveal a cortico-brainstem-thalamic circuit that controls motor activity. Glycinergic PRF neurons (**GlyT2+**) receive motor cortical inputs, which also target the thalamus and the basal ganglia, forming a regulatory loop. In turn, **GlyT2+** PRF neurons inhibit the ipsilateral thalamus and medulla and drive contralateral turning.

Highlights

- Motor cortex targets thalamic-projecting PRF/GlyT2+ cells and control their activity
- PRF/GlyT2+ cells inhibit the ipsilateral IL/Pf in the thalamus and also target the medulla
- Activation of IL/Pf-projecting PRF/GlyT2+ cells induces contralateral turning
- Ipsilateral PRF inhibition and contralateral excitation act synergistically on turning



Article

A cortico-subcortical loop for motor control via the pontine reticular formation

Emília Bósz,^{1,2,6,7} Viktor M. Plattner,^{1,3,6} László Biró,^{1,6} Kata Kóta,^{1,4} Marco A. Diana,⁵ and László Acsády^{1,7,*}

¹Lendület Thalamus Research Group, HUN-REN Institute of Experimental Medicine, 1083 Budapest, Hungary

²János Szentágothai Doctoral School of Neurosciences, Semmelweis University, 1083 Budapest, Hungary

³Sainsbury Wellcome Ctr., London W1T 4JG, UK

⁴Semmelweis University, 1083 Budapest, Hungary

⁵Université Paris Cité, CNRS, Saint-Pères Paris Institute for the Neurosciences, 75006 Paris, France

⁶These authors contributed equally

⁷Lead contact

*Correspondence: acsady@koki.hu

<https://doi.org/10.1016/j.celrep.2025.115230>

SUMMARY

Movement and locomotion are controlled by large neuronal circuits like the cortex-basal ganglia (BG)-thalamus loop. Besides the inhibitory thalamic output, the BG directly control movement via specialized connections with the brainstem. Whether other parallel loops with similar logic exist is presently unclear. Here, we demonstrate that the secondary motor and cingulate cortices (M2/Cg) target and strongly control the activity of glycine transporter 2-positive (GlyT2+) cells in the pontine reticular formation (PRF). In turn, PRF/GlyT2+ cells project to and powerfully inhibit the intralaminar/parafascicular nuclei of the thalamus (IL/Pf). M2/Cg cells co-innervate PRF/GlyT2+ cells and the IL/Pf. Thalamus-projecting PRF/GlyT2+ cells target ipsilateral subcortical regions distinct from BG targets. Activation of the thalamus-projecting PRF/GlyT2+ cells leads to contralateral turning. These results demonstrate that the PRF is part of a cortico-subcortical loop that regulates motor activity parallel to BG circuits. The cortico-PRF-thalamus loop can control turning synergistically with the BG loops via distinct descending pathways.

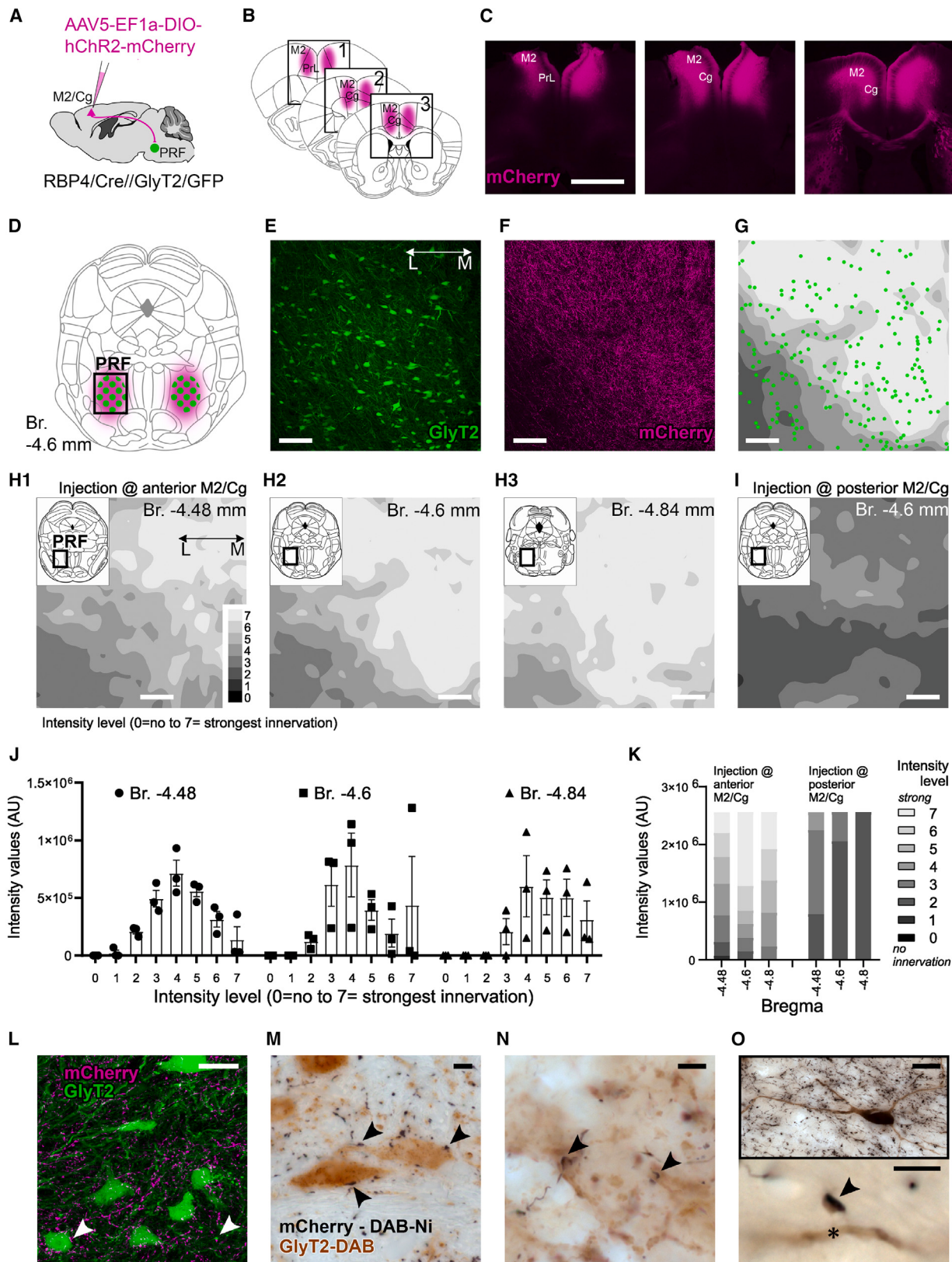
INTRODUCTION

Voluntary movements are controlled via diverse cortical and subcortical centers.^{1,2} Among these, the basal ganglia (BG) are one of the most intensively studied and are thought to be responsible for the planning, execution, and learning of complex motor sequences.^{2–5} Two key features characterize the BG circuits. First, cortex, BG, and thalamus are engaged in the formation of complex loops^{6–8}; second, the output of these loops is communicated as a strong inhibitory signal to brainstem locomotor centers via the BG output nuclei.^{9,10}

The cortex-BG-thalamus loop can be regarded as a multiple-nested loop^{11–13} since the cortical signals return to the cortex via both the direct, thalamo-cortical projections and via an indirect loop that passes through the BG and the thalamus.^{6–8} Since the entire system is strongly topographical the indirect BG signals and the direct cortico-thalamic pathway are integrated in the same thalamic territory.^{6,8,14} This pattern of connectivity is especially useful to generate multiple embedded rhythms, the hallmark of cortical and brainstem activity governing locomotion.¹ Individual cortical neurons can provide axon collaterals to both the direct thalamo-cortical pathway^{15–17} and the indirect cortex-BG loop, ensuring that an identical cortical message is transferred via these two nested pathways.

How the cortex-BG-thalamus loop communicates with the brainstem locomotor centers has been poorly investigated until recently. By now it appears that the BG innervate multiple brainstem locomotor centers and can have a strong impact on their activity.⁹ A recent study¹⁰ has demonstrated a specific role of the BG in regulating turning behavior via the pontine reticular formation (PRF) (its rostral part also referred to as nucleus pontis oralis). PRF has already been implicated earlier in motor control.^{18,19} Cregg et al.¹⁰ showed that the substantia nigra pars reticulata (SNR), a major output nucleus of the BG, can effectively inhibit the excitatory vesicular glutamate transporter 2 (vGLUT2)-containing neurons in the PRF. These PRF/vGLUT2+ neurons, in turn, innervate the contralateral gigantocellular nucleus (Gi) in the lower brainstem. Gi cells can mediate ipsiversive turning and motor arrest via their direct reticulo-spinal connections.^{20,21} The new study shows that decreased inhibitory SNR output results in increased PRF/vGLUT2+ output, which consequently elevates contralateral Gi activity leading to a contralateral turning, relative to the side of SNR-PRF interaction. Increased BG output has the opposite effect.¹⁰ Modulating the PRF/vGlut2+-Gi pathway restores turning ability after striatal damage, implying that impairment in this pathway could contribute to the disabling turning deficits associated with Parkinson's disease.¹⁰ These data demonstrate how the output of the cortex-thalamus-BG loop can have direct





(legend on next page)

behavioral consequences via modulating the activity of the brainstem motor centers.

Curiously, the BG output avoided the other major cell type of the PRF, the equally numerous inhibitory, glycine transporter 2-expressing cells (PRF/GlyT2+ cells).^{10,22} At the same time, however, Gi neurons, ipsilateral to the turning, receive a strong inhibition,¹⁰ the sources of which are unknown. PRF/GlyT2+ neurons have dual GABAergic/glycinergic phenotype and can innervate the same thalamic regions (the intralaminar/parafascicular nuclei [IL/Pf]) as the BG-thalamic pathway.²³ IL/Pf have already been also implicated in movement coordination, turning, and orienting behavior.^{24–26} The thalamic-projecting PRF/GlyT2+ cells establish large, highly effective multisynaptic inhibitory terminals, very similar to those of the BG terminals in the thalamus.^{23,27} PRF is known to receive input from higher-order motor cortical areas^{28,29} and photoactivation of thalamus-projecting PRF/GlyT2+ cells results in motor arrest.²³ These data indicate that, even though PRF/GlyT2+ cells are not innervated directly by the BG output, they may participate in an independent cortico-thalamic loop and can contribute to motor control.

Based on these data, in this study, we tested whether thalamic-projecting PRF/GlyT2+ neurons can represent a brainstem movement control system involved in a nested loop organization with the cortex and thalamus that can contribute to turning behavior. Our data demonstrate that thalamus-projecting PRF/GlyT2+ cells receive strong cortical excitatory inputs, via cortical layer 5 (L5) neurons. L5 neurons, in addition to innervating the PRF, also arborize in the IL/Pf, the target of PRF/GlyT2+ cells. We also show that thalamic-projecting PRF/GlyT2+ cells can evoke pronounced inhibitory action on their thalamic targets and affect turning behavior synergistically with the PRF/vGLUT2+ cells via a selective ipsilateral projection to Gi.

RESULTS

M2/Cg cortical neurons innervate PRF/GlyT2+ neurons

To visualize cortical inputs to PRF/GlyT2+ neurons, we used anterograde virus-mediated tracing in RBP4-Cre//GlyT2-eGFP double transgenic mice. RBP4 is known to be expressed in deep L5 pyramidal cells that project to subcortical targets.³⁰

Figure 1. Cortical inputs to PRF/GlyT2+ cells

- (A) Scheme of anterograde tracing from the frontal cortical motor-related areas (M2/Cg) in the RBP4-Cre//GlyT2-eGFP mouse line ($n = 9$ mice).
- (B) Schematic view of the injection sites.
- (C) Low-power fluorescent micrographs of the cortical injection sites at three anteroposterior levels.
- (D) Schematic view of the M2/Cg fibers (magenta shade) and PRF/GlyT2+ cells (green dots). The black rectangle, the position of the micrographs, and heatmaps in (E)–(G).
- (E and F) Confocal micrographs ($n = 5$ mice) of the glycinergic cells (E) and anterogradely labeled M2/Cg cortical fibers (F) in the PRF glycinergic zone.
- (G) Fiber density heatmap showing the distribution of cortical fibers (gray shading) and PRF/GlyT2+ cells (green dots). Higher fiber density is indicated with light gray colors.
- (H1–3) Maximum intensity Z projections of average cortical fiber heatmaps ($n = 3$ animals) showing anterior M2/Cg inputs at three anteroposterior PRF levels extending from Br. –4.6 to Br. –4.84 (from the Paxinos atlas; 250 μm).
- (I) Maximum intensity Z projections of cortical fiber heatmaps ($n = 3$ animals) showing posterior M2/Cg inputs.
- (J) Quantitative analysis of the anterior M2/Cg fibers in the PRF at three coronal levels. Intensity levels represent fiber density values between 0 and 7, where 0 indicates no innervation and 7 presents the strongest innervation.
- (K) Proportion of innervation densities in the PRF after anterior (left) and posterior (right) M2/Cg injections at three coronal levels.
- (L) High-power confocal fluorescent image of anterogradely labeled M2/Cg fibers (magenta) and PRF/GlyT2+ neurons (60 \times , $n = 5$ mice).
- (M–O) High-power light microscopic image ($n = 9$ mice) of close apposition between M2/Cg fibers (black) and the somata (K), dendrites (L), or a spine (M) of PRF/GlyT2+ neurons. Inset in (M) displays the juxtacellularly labeled PRF/GlyT2+ cell; arrowheads, cortical inputs; asterisk, spine. Scale bars, 1 mm (C), 100 μm (E–I), 20 μm (J), 5 μm (M), 5 μm (K and L), 20 μm (inset).

We injected AAV5-DIO-ChR2-mCherry virus into the secondary motor/cingulate (M2/Cg) cortical area since these regions are known to contain the highest concentration of PRF-projecting cells²³ (Figures 1A–1C). GlyT2+ cells were detected by the eGFP expression.²² Anterogradely labeled M2/Cg fibers formed a profuse axon arbor within the entire rostral PRF (Figures 1D–1F). The distribution of cortical afferents displayed significant overlap with that of the PRF/GlyT2+ neurons (Figures 1D–1F) but was not homogeneous within the PRF. A density map of cortical afferents showed a dorsomedial to ventrolateral decrease in fiber density within the PRF/GlyT2+ zone (Figures 1G and S1A–S1C). This gradient was present at all coronal levels examined on averaged maximum intensity projection of the fiber density maps in three animals (Figures 1H1–1H3 and S1A–S1C). Caudal injections into the M2/Cg cortex ($n = 3$) resulted in weaker PRF innervation (Figure 1I). The quantitative analysis of intensity levels showed that the whole PRF was innervated by M2/Cg (Figure 1J). The posterior M2/Cg afferents displayed low-intensity levels (2–4) compared with the anterior M2/Cg innervation where we observed higher fiber density (intensity levels 1–7, Figure 1K).

Next, we visualized anterior M2/Cg fibers and PRF/GlyT2+ neurons using high-power confocal imaging and high-power light microscopy using DAB/Ni (black) and DAB (brown) chromogens. With both methods, and cortical afferents were in close proximity to PRF/GlyT2+ elements (Figure 1L). We found putative synaptic contacts on the dendrites and occasionally on the somata of GlyT2+ neurons (Figures 1M and 1N). In one case the spine of a PRF/GlyT2+ neuron, filled using the juxtacellular labeling method (see below), was found to be contacted by an M2/Cg cortical terminal (Figure 1O).

To identify the synaptic contacts formed by M2/Cg terminals in the PRF, we analyzed the ultrastructure of the M2/Cg synapses at the electron microscopic level (Figures 2A–2D). M2/Cg terminals were small to medium-sized (mean = 0.47 μm^2 SD = 0.31, Figures 2B–2D and S1D), contained 1–3 mitochondria, and established asymmetrical synapses with 1–2 active zones mainly with dendrites (range: 0.197–1.437 μm , mean = 0.62 μm , SD = 0.31, Figures 2B–2D). The postsynaptic elements have variable diameters. Using double immunocytochemistry we identified

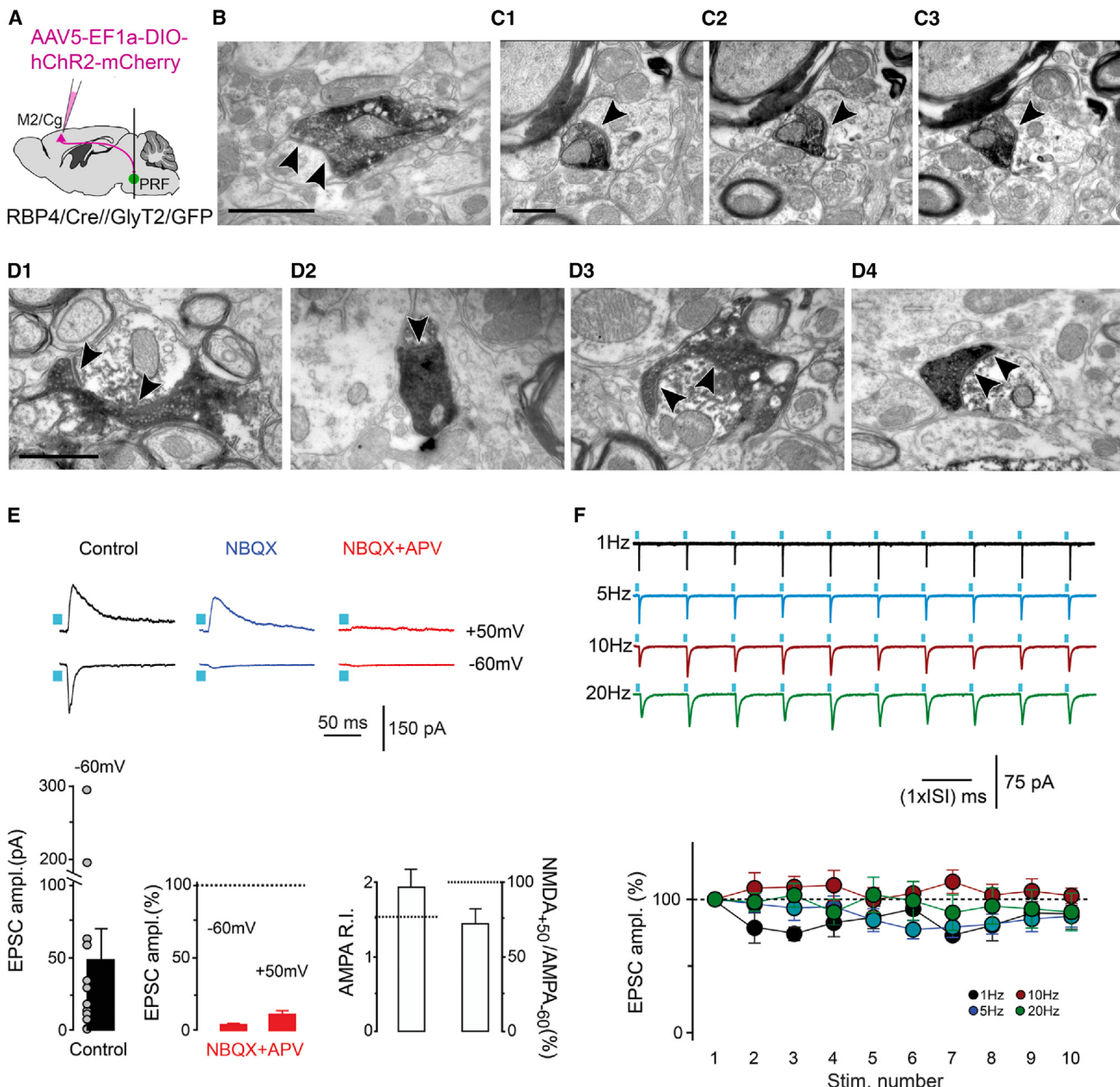
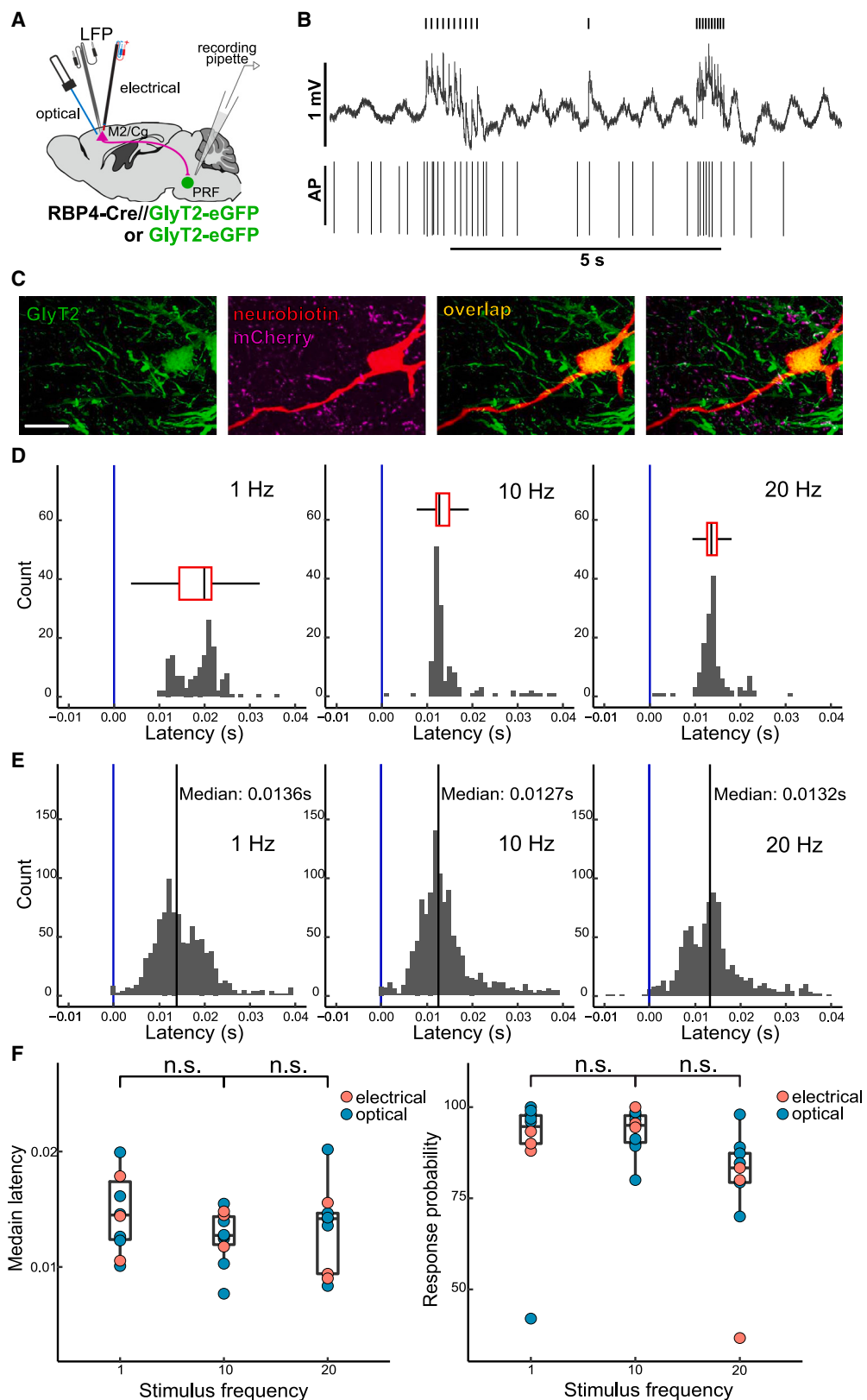


Figure 2. Cortical afferents target PRF/GlyT2+ cells and evoke a glutamatergic synaptic response

- (A) Scheme of anterograde tracing from the M2/Cg in the RBP4-Cre//GlyT2-eGFP mouse line.
- (B and C) Electron micrographs of M2/Cg terminals ($n = 44$, dark precipitates) in the PRF-contacting mid-caliber dendrites.
- (C1-C3) Serial EM images of the same axon terminal. Black arrowheads, synapses.
- (D) Electron micrographs of M2/Cg terminals (DAB-Ni, dark, dense precipitate) establishing synapses on PRF/GlyT2+ dendrites ($n = 9$, D1, D3, D4, DAB, light precipitate) and spines ($n = 1$, D2).
- (E) Optogenetically evoked (blue squares) AMPA and NMDA receptor-mediated components of the EPSCs elicited by M2/Cg terminals in the PRF. Traces from one exemplary experiment are shown above. Top: AMPA and NMDA components ($n = 16$), control at -60 mV ($n = 12$; $p = 0.002$; Wilcoxon signed-rank test) and $+50$ mV ($n = 12$; $p = 0.003$; Wilcoxon signed-rank test). Below, the graphs represent the results from all the experiments.
- (F) Top: light-evoked EPSC-s displayed no significant depression during stimulation trains, at all tested frequencies ranging from 5 to 20 Hz. Bottom: $89.1\% \pm 11.5\%$ ($n = 6$; $p > 0.05$; Wilcoxon signed-rank test), $87.3\% \pm 8.2\%$ ($n = 14$; $p = 0.03$; Wilcoxon signed-rank test), $102.7\% \pm 5.7\%$ ($n = 10$; $p = 0.7$; Wilcoxon signed-rank test), $90.5\% \pm 14.0\%$ ($n = 12$; $p = 0.1$; Wilcoxon signed-rank test) at 1, 5, 10, and 20 Hz, respectively. Source data are provided as a Source Data file. Data are represented as mean \pm SE. Scale bars: 1,000 nm (B), 500 nm (C), 1,000 nm (D).



(legend on next page)

synaptic contacts between virus-labeled cortical afferents and PRF/GlyT2+ neurons in 10 cases (Figure 2D1–2D4). In 9 cases the postsynaptic structure was a mid-caliber dendrite, in 1 case it was a PRF/GlyT2+ spine. These data show that the anterior M2/Cg provides a dense innervation to the PRF, which contains GlyT2+ neurons and forms conventional synaptic contacts mainly with the dendrites of GlyT2+ neurons in the PRF.

Synaptic properties of the cortical inputs in PRF/GlyT2+ neurons

Next, we investigated the physiology of synapses formed by the cortico-PRF terminals in GlyT2+ cells. *In vitro*, PRF slice preparations were made from RBP4-Cre//GlyT2-eGFP animals that received identical AAV5-DIO-ChR2-mCherry M2/Cg injections as in the case of the anterograde tracing experiments. Optogenetic activation with brief flashes (2–3 ms) of blue light-evoked synaptic responses. At a recording potential of -60 mV, these triggered rapidly rising and decaying inward synaptic currents with an averaged amplitude amounting to 48.6 ± 20.2 pA (Figure 2E, bottom panel). The amplitude of these responses was not modified by bath application of the GABAergic/glycinergic synaptic blockers SR95531 ($2 \mu\text{M}$) and strychnine ($10 \mu\text{M}$), thus demonstrating their excitatory nature. When recorded at a holding potential of $+50$ mV (see STAR Methods), the EPSCs showed clearly slower decaying kinetics than at -60 mV, consistently with the appearance of an N-methyl D-aspartate (NMDA) receptor-mediated component at the depolarized potential (Figure 2E, top panel, blue traces). Bath co-application of NBQX ($10 \mu\text{M}$) and DL-APV ($50 \mu\text{M}$), led to almost complete inhibition of the synaptic responses to $5.6\% \pm 1.4\%$ of the control at -60 mV, and to $10.1\% \pm 3.0\%$ at $+50$ mV (Figure 2E, top red traces), thus demonstrating the glutamatergic nature of the cortico-PRF/GlyT2+ inputs. The amplitude of the NMDA component, as measured at $+50$ mV, amounted to $68.7\% \pm 15.3\%$ of the α -amino-3-hydroxy-5-methyl-4-isoxazolepropionic acid (AMPA) component at -60 mV (Figure 2E). Moreover, the AMPA rectification index (measured as the ratio between the AMPA component amplitudes at -60 and $+50$ mV) amounted to 1.9 ± 0.3 ($n = 17$; Figure 2E, bottom), not distant from the theoretical value of 1.75 for a linear I-V curve. This strongly suggests that the AMPA receptors present at these synapses are calcium-impermeable in PRF/GlyT2+ neurons.

In control pharmacological conditions, we examined the dynamic behavior of the cortico-PRF glutamatergic responses with trains of 10 optogenetic stimulations at different frequencies

(1 , 5 , 10 , and 20 Hz). Along the stimulation trains the synaptic responses in the PRF/GlyT2+ cells did not show a significantly depressing behavior, the amplitude of the responses to the 10th stimulation being significantly smaller than the one to the first light pulse only at 5 Hz (see top traces in Figure 2F). With respect to the first optogenetic stimulation, the amplitudes of the responses to the 10th light pulse were indeed $89.1\% \pm 11.5\%$, $87.3\% \pm 8.2\%$, $102.7\% \pm 5.7\%$, and $90.5\% \pm 14.0\%$ at 1 , 5 , 10 , and 20 Hz, respectively (see bottom graph in Figure 2F). These data demonstrate that the cortical inputs to the PRF/GlyT2+ neurons identified morphologically exert a pronounced, conventional, purely glutamatergic synaptic action with little short-term depression.

The impact of cortical activation on PRF/GlyT2+ neuronal activity

To assess the impact of cortical inputs on the spiking activity of PRF/GlyT2+ neurons *in vivo*, we recorded the evoked responses of the PRF cells in ketamine-xylazine anesthetized animals ($n = 10$ animals, Figure 3). In 7 cases we injected the AAV5-DIO-ChR2-mCherry virus into M2/Cg in the RBP4-Cre//GlyT2-eGFP double transgenic mice and photostimulated the L5 neurons (Figures 3A and 3B). In 3 cases we applied bipolar electrical stimulation of the cortex in GlyT2/GFP transgenic mice (5 ms pulse width, $1\text{--}2$ mA). In both stimulating conditions, we used trains of 1 , 10 , and 20 Hz stimulations ($n = 50$ stimulus in 5 trains, Figure S2). To unequivocally identify and localize PRF/GlyT2+ neurons we used the juxtacellular recording and labeling methods.³¹ Nine out of 10 neurons were recovered post hoc within the PRF and their GlyT2+ identity was determined by double fluorescent imaging (Figure 3C and S2A).

Cortical stimulation at 1 Hz generated reliable spike responses with short latency peaks in all PRF/GlyT2+ cells (Figures 3D and 3E) using both stimulation methods. Increasing the stimulation frequency to 10 and 20 Hz resulted in similar high-fidelity, fast responses (Figures 3D and 3E). We found no significant difference between stimulation frequencies in response probability and latency (Figure 3F), indicating reliable signal transmission even at high presynaptic activity. To assess the alteration of firing output of the PRF/GlyT2+ cells within the stimulation train at various input frequencies, we calculated the normalized evoked action potentials (AP) within a 50 ms time window after every stimulus (Figure S2B). The data demonstrated that the spiking activity of individual PRF/GlyT2+ cells did not depress within the stimulus train irrespective of the stimulation frequencies (Figure S2B).

Figure 3. The effect of evoked cortical activity on PRF/GlyT2+ neurons

- (A) Scheme of the experiments ($n = 10$ mice: 7 mice with optogenetic 5-ms-long pulses at $1\text{--}20$ mW [RBP4-Cre//GlyT2-eGFP], 3 mice with electrical 5 ms pulses at $1\text{--}2$ mA [GlyT2-eGFP]).
- (B) Representative stimulus-evoked cortical field activity and evoked firing of a glycinergic PRF neuron. Small ticks on the top indicate laser stimulation.
- (C) Representative fluorescent micrograph of a recorded and labeled PRF/GlyT2+ neuron. Green, GlyT2-eGFP; red, neurobiotin; magenta, M2/Cg fibers.
- (D) Peristimulus time histograms (PSTH) of cortical stimulus-evoked firing in a representative PRF/GlyT2+ neuron at 1 , 10 , and 20 Hz stimulation frequencies. Response probability and median latency are visualized by boxplots. 1 Hz: probability 92.86% , 12.5 ms peak \pm SEM; 10 Hz: probability: 92.86% , 12.6 ms peak \pm SEM, 20 Hz: probability 84.06% , 14.5 ms peak \pm SEM.
- (E) Population PSTHs of juxtacellularly recorded and labeled PRF/GlyT2+ neurons ($n = 10$) at 1 , 10 , and 20 Hz. 1 Hz median: 0.0136 s; 10 Hz median: 0.0127 s, 20 Hz median: 0.0132 s.
- (F) Median latency (left) 1 vs. 10 Hz, n.s. $p = 0.22$; 10 Hz vs. 20 Hz n.s. $p = 0.3$, Mood's median test and response probability (right) 1 vs. 10 Hz, n.s. $p = 0.59$; 10 Hz vs. 20 Hz n.s. $p = 0.65$ Mood's median test of the PRF/GlyT2+ neurons. * $p < 0.05$, ** $p < 0.01$, *** $p < 0.001$; n.s., no significant difference. Source data are provided as a Source Data file. Scale bars, $20 \mu\text{m}$ (C).

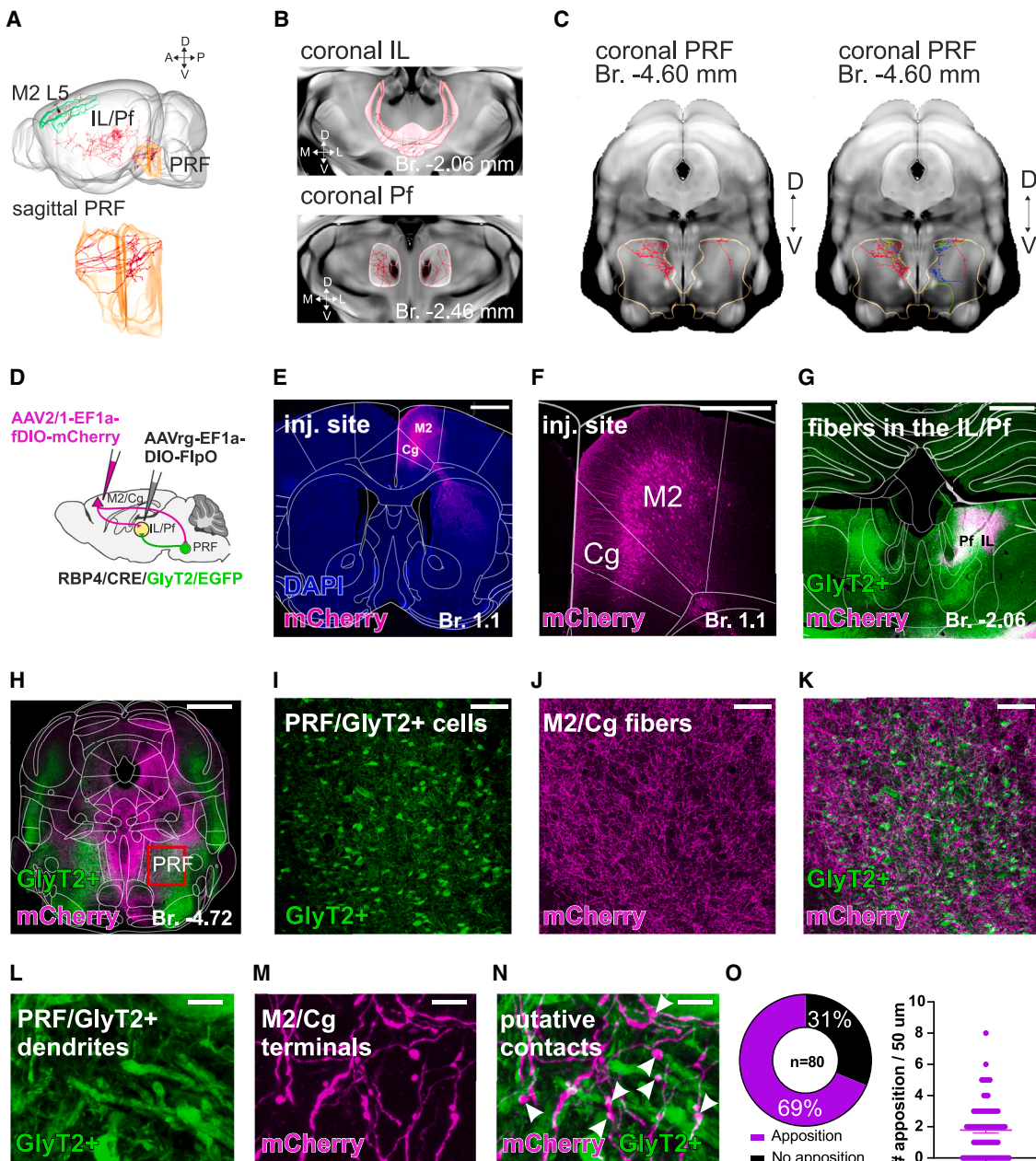


Figure 4. Co-innervation of PRF and thalamus by M2/Cg L5 neurons

- (A) Reconstruction of a representative M2 L5 (AA0245) neuron from the Mouse Light Neuron Browser database which innervates both PRF and IL/Pf (top). Axon arbor of the representative M2 L5 neuron (AA0245) at the sagittal level in the PRF (bottom).
- (B) Axon arbor of the representative M2 L5 neuron (AA0245) in the IL (top) and Pf (bottom).
- (C) Axon arbor of the representative M2 L5 neuron (AA0245) (left in red) and of 4 L5 neurons in the PRF (right, red, yellow, blue, and green) that have 10 or more axonal endpoints in the PRF and also innervate IL/Pf with multiple endpoints.
- (D) Scheme of the viral tracing to label PRF collaterals of thalamus-projecting M2/Cg cells.
- (E) Low-power confocal micrograph of the cortical M2/Cg injection site.
- (F) High-power confocal fluorescent image of the thalamus-projecting M2 L5 neurons.
- (G) Merged confocal image of the labeled thalamus-projecting M2/Cg cortical fibers (magenta) and PRF/GlyT2+ fibers (green) in the thalamus.
- (H) Merged, low-power confocal image of the labeled thalamus-projecting M2/Cg cortical fibers (magenta) and PRF/GlyT2+ fibers (green) in the brainstem.
- (I–K) Confocal micrographs of the PRF/GlyT2+ cells (green, I), anterogradely labeled thalamus-projecting M2/Cg cortical fibers (magenta, J), and their merged image (K).

(legend continued on next page)

These *in vivo* data confirm the *in vitro* physiological data and show that frontal cortical cells can evoke fast, reliable spike responses in PRF/GlyT2+ cells even at high presynaptic stimulation frequencies.

Impact of spontaneous cortical activity on PRF/GlyT2+ cells

Earlier data indicated that the activity of PRF/GlyT2+ cells can be linked to different phases of slow cortical oscillations.²³ Here, we asked to what extent the firing activity of PRF/GlyT2+ cells is sensitive to the alterations of cortical states (synchronized vs. desynchronized, Figures S3 and S4A–S4C). We recorded PRF/GlyT2+ neurons ($n = 12$) in GlyT2-eGFP transgenic animals and monitored the state changes in local field potential (LFP) activity (Figures S3A and S3B). In the case of seven cells, we recorded spontaneous state changes between synchronized and desynchronized cortical states, which can be observed in light ketamine-xylazine anesthesia (Figure S3B), whereas in five cases we evoked cortical inactivity by applying 2 M potassium chloride (KCl) to the cortical surface to induce cortical spreading depression (CSD) (Figures S4D–S4F).³²

In the first experiments, we observed that five out of seven PRF/GlyT2+ cells fired rhythmic AP clusters during the slow oscillatory periods (Figures S3B–S3D and S4A). When the slow oscillation was replaced by a desynchronized period in the LFP, the firing pattern of the PRF/GlyT2+ cells immediately followed this transition and became irregular (Figures S3B–S3D and S4A). When the rhythmic cortical activity was restored, the AP clusters reappeared (Figures S3B–S3D and S4C). The transition from rhythmic AP cluster to tonic activity could be confirmed by autocorrelograms (Figures S3C and S4A). The mean rate of PRF/GlyT2+ action potential clusters was significantly higher in synchronized vs. desynchronized states (Figure S3D). The firing rate of PRF/GlyT2+ neurons significantly increased during the desynchronized states (Figure S4B). In the CSD experiments, cells decreased the rate of spike clusters upon cortical cell inactivation (Figure S4F). These data demonstrate a tight connection between the cortical states and firing activity of PRF/GlyT2 neurons and confirm the strong impact of the cortex on these cells during spontaneous activity.

Co-innervation of PRF and the thalamic targets of PRF by L5 neurons

L5 neurons that innervate the striatum have been shown to arborize in the thalamus^{15,16} and since the basal ganglia also innervate the thalamus and thalamus project back to the cortex the three structures form multiple nested loops.^{6,8,11}

To investigate if the same logic applies to individual L5 neurons targeting the PRF, i.e., whether L5 neurons simultaneously innervate PRF and the target region of PRF/GlyT2+ cells in the thalamus (the IL/Pf) we analyzed data from the Mouse Light Neuron Browser database³³ (<https://www.janelia.org/open-science/mouselight-neuronbrowser>). In the database we

found 23 M2/Cg L5 neurons that had at least one axonal endpoint in the PRF (Figures 4A–4C; Table S1). Seventy-four percent of these neurons ($n = 17$) projected to the IL/Pf as well. Ten out of the M2/Cg L5 17 neurons (59%) co-innervating PRF and IL/Pf displayed multiple axonal endpoints (here defined as more than 4 endpoints) both in PRF and in the IL/Pf. Four out of the 23 PRF-projecting L5 neurons (17.4%) displayed very dense axonal arbors in PRF (more than 10 axonal endpoints) (Figure 4C). Three of these L5 cells innervated IL/Pf also with more than 10 axonal endpoints. The fourth of them formed 6 endpoints in IL/Pf. Confirming our anterograde tracing experiments, these neurons arborized more in the dorsomedial part of the PRF (Figure 4C). These data suggest that co-innervation of PRF and IL/Pf by individual cortical L5 neurons is common. Sixteen out of the 17 L5 neurons (94.12%) co-innervating PRF and IL/Pf also had a collateral to the striatum indicating that the cortico-PRF-thalamic message is projected to the basal ganglia as well (Table S1).

The Mouse Light Neuron Browser data do not permit to establish whether the cortico-PRF-thalamic neurons target PRF/GlyT2+ cells or other cell types in the PRF. To demonstrate that thalamic-projecting cortical cells can innervate PRF/GlyT2+ cells, we employed two experimental designs (Figure 4D and S5A). In the first configuration, we injected AAVrg-EF1a-DIO-FlpO into the IL/Pf and AAV2/1-EF1a-fDIO-mCherry into M2 in RPB4-Cre//GlyT2-eGFP mice (Figure 4D). In this case, the Flp is Cre dependent, travels retrogradely from the thalamus to the cortex, and expresses in RBP4+ L5 neurons (Figures 4E and 4F). The second virus is FLP dependent and travels anterogradely from those L5 neurons, which project to the IL/Pf as well (Figures 4G–4K). In the second approach, we injected Cre-expressing retrograde virus (AAVrg-EF1a-Cre) into the IL/Pf and AAV5-EF1a-DIO-hChr2-mCherry virus into the M2 in GlyT2-EGFP mice (see more details in the STAR Methods; Figure S5A).

In both experimental approaches, we observed retrogradely labeled deep layer M2/Cg pyramidal cells (Figures 4F, S5B and S5C) and dense axonal arbor in the dorsolateral Pf/IL verifying the injection sites and the thalamic projections (Figures 4G, S5D–S5H, and S5M–S5P). Dense cortical innervation was also observed in the PRF in every case ($n = 4$ animals) in the same PRF/GlyT2+ area (Figures 4H–4K and S5I–S5L), which we identified after our original M2/Cg AAV5-DIO-ChR2-mCherry injections (as in Figure 1). The cortical projection was largely ipsilateral in the PRF. Using high-resolution confocal microscopy, we identified close appositions between axons of IL/Pf-projecting cortical neurons and the dendrites of PRF/GlyT2+ cells (Figures 4L–4N). In the first experimental configuration, 72.5% of PRF/GlyT2+ dendrites ($n = 40$) were contacted by the axon terminals of thalamic-projecting M2/Cg axons, compared with 65% in the second experiment ($n = 40$). The mean number of close appositions per dendrite was 2.125 ± 0.308 in the first case and 1.45 ± 1.339 in the second. The pooled data show that 69% of

(L–N) High-power confocal microscopic image of close apposition between the PRF/GlyT2+ dendrites (green, L) and thalamus-projecting M2/Cg fibers (magenta, M). Arrows, putative contacts in (N).

(O) Percentage of innervated PRF/GlyT2+ dendrite (left) and the mean number of the close apposition per dendritic segment (right). Source data are provided as a Source Data file. Scale bars, 1 mm (E), 500 μ m (F and G), 1 mm (H), 100 μ m (I–K), 5 μ m (L–N).

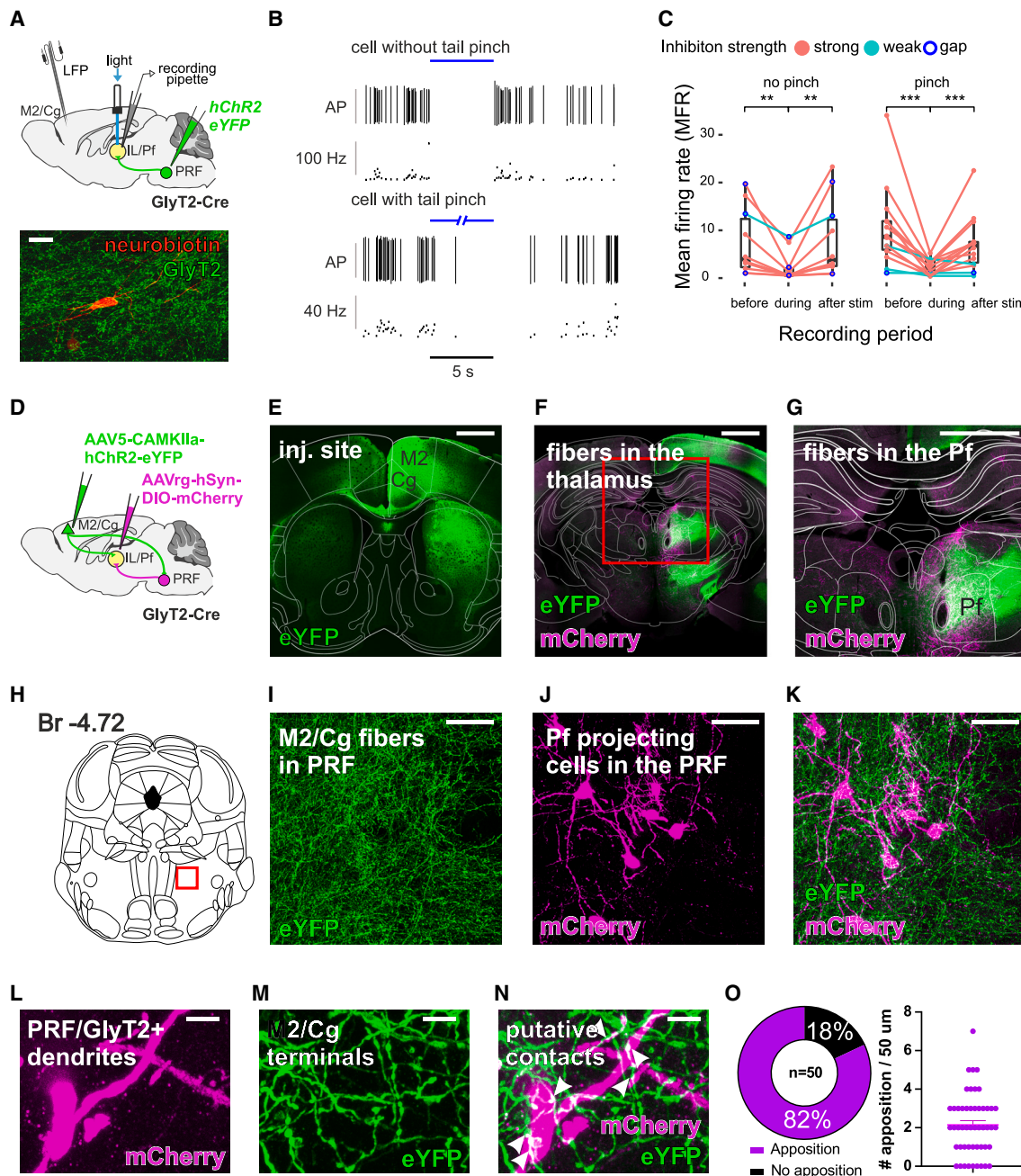


Figure 5. Inhibitory action and cortical innervation of thalamus-projecting PRF/GlyT2+ cells

(A) Top: scheme of the juxtacellular recordings ($n = 13$ mice, $n = 23$ neurons). Bottom: post hoc identified IL/Pf neuron surrounded by GlyT2+ fibers.

(B) Response of two representative IL/Pf thalamic neurons to optogenetic activation of PRF/GlyT2+ fibers (top, 5 s stimulation, without a tail pinch; bottom, 30 s stimulation with a tail pinch). Top: discriminated action potentials (AP), 5 s stimulation, without tail pinch. Bottom: instantaneous firing rate (blue line, laser ON), 30 s stimulation with a tail pinch.

(C) Mean firing rate (MFR) of the recorded IL/Pf thalamic neurons before, during, and after the photoactivation PRF/GlyT2+ fibers (33 Hz, 5 ms pulse width, laser power 10 mW, 5–30 s duration). Strongly inhibited, (red circles, $n = 19$ cell), weakly inhibited (light blue circles, $n = 4$, see STAR Methods) and neurons responding with a post-stimulus gap (dark blue circle, $n = 4$) are indicated. No pinch (left) and pinch (right) conditions are shown separately. No pinch MFR before vs. stim $p = 0.002$; no pinch MFR stim vs. after $p = 0.002$, $n = 10$ cells; pinch before vs. stim $p = 0.00012$; pinch MFR stim vs. after $p = 0.00085$, $n = 14$ cells; Wilcoxon signed-rank test.

(D) Scheme of the double conditional viral tracing to label cortical inputs to thalamus-projecting PRF/GlyT2+ cells.

(E) Low-power confocal micrograph of the cortical injection site.

(legend continued on next page)

the PRF/GlyT2+ dendritic segments ($n = 80$) were juxtaposed to M2/Cg boutons, with an average of 1.45 ± 1.339 putative contacts per 50 μm segment (Figure 4O). Together these data show that thalamus-projecting M2/Cg pyramidal cells can also innervate PRF/GlyT2+ cells.

Activation of PRF/GlyT2+ neurons inhibits thalamocortical neuronal activity *in vivo*

As the next step in the loop, we aimed to examine the impact of PRF/GlyT2+ activity on thalamic cells. PRF/GlyT2+ neurons have been shown to selectively innervate IL/Pf and evoke non-depressing, mixed, GABA/glycine receptor-mediated IPSCs on their targets.²³ However, the effect of this inhibitory input on the spike output of IL/Pf has not been investigated. To address this, we performed *in vivo* juxtacellular recording and labeling experiments in GlyT2-Cre mice injected with an AAV5-DIO-ChR2-eYFP virus in the PRF (Figures 5 and S6). PRF/GlyT2+ fibers were then photoactivated in the IL/Pf (Figure 5A and 5B). To ensure that the recorded IL/Pf neurons were located within the PRF/GlyT2+ fibers, the position of the IL/Pf cells was determined post hoc (Figure S6A). Given that IL/Pf neurons are known to be sensitive to pain³⁴ we utilized urethane anesthesia to assess the impact of PRF/GlyT2+ photoactivation on spontaneous ($n = 13$ cells) as well as on tail-pinch-induced IL/Pf activity ($n = 10$ cells; Figures 5B, 5C, S6B, and S6C). The stimulation frequency used (33 Hz) was compatible with the spontaneous activity of PRF/GlyT2+ neurons measured under identical conditions.²³

The baseline mean firing rate (MFR) of the recorded thalamic neurons ($n = 23$) varied between 1 and 30 Hz (Figure S6B). Tail pinch evoked a significantly higher MFR in the IL/Pf cells (Figure S6B). Optogenetic activation of PRF/GlyT2+ fibers (33 Hz) in the IL/Pf resulted in a significant decrease of IL/Pf spiking activity in both spontaneous and tail-pinch conditions at the population level (Figures 5B, 5C, S6C, and S6D). The firing rate immediately returned to baseline values upon the cessation of stimulus trains (Figure 5B, 5C, S6C, and S6D).

Nineteen out of the 23 IL/Pf neurons (82.6%) were considered strongly inhibited (see STAR Methods; Figure S6E). In these neurons, inhibition of the firing output increased gradually and following a transient period of 1–2 s PRF/GlyT2+ inputs could almost entirely block the firing output of IL/Pf cells (Figures S6D and S6E). In 9 neurons we increased the duration of stimulation from 5 to 16 or 30 s but the tonic cessation of firing was maintained for the entire duration ($n = 9$ cell, Figure S6D). Firing activity returned to baseline levels after these long stimulations as well (Figure S6D). In the case of 4 out of the 23 IL/Pf neurons (16.7%), the PRF/GlyT2+ activation resulted in a brief

gap (5–10 ms) in the PSTH immediately after the onset of the stimulus (Figures S6F and S6G). The time course of this precisely timed inhibition corresponded well with the kinetics of the fast GABAergic/glycinergic IPSCs recorded during the earlier *in vitro* observations²³ indicating a fast, phasic inhibition in this subset of neurons. The activity of control neurons in the thalamus, located outside the PRF/GlyT2+ projection zone ($n = 5$), was not altered by the activation of PRF/GlyT2+ fibers (Figures S6D and S6H).

The precise localization of IL/Pf neurons inhibited by PRF/GlyT2+ activation was verified post hoc. IL/Pf cells were localized within the PRF/GlyT2+ fibers in all cases (Figure S6A), mainly in the dorsolateral sectors. The recorded cells were distributed both in the anterior (centrolateral and paracentral) and the posterior (parafascicular) IL nuclei (Figure S6A). All weakly inhibited cells were localized in the anterior IL. We conclude that PRF/GlyT2+ neurons can exert a powerful effect on the spontaneous as well as on tail-pinch-evoked firing activity of IL/Pf neurons and can participate in both tonic (divisive) and phasic inhibition of IL/Pf outputs.

So far, we have shown that the cortico-PRF pathway can effectively control PRF/GlyT2+ cells (Figures 3 and S2–S5) and that, in turn, PRF/GlyT2+ cells can strongly inhibit their postsynaptic partner in the thalamus (Figure 5 and S6). However, it still remains to directly demonstrate whether cortical L5 axons can actually target those PRF/GlyT2+ neurons, which innervate the thalamus and inhibit IL/Pf neurons. To investigate this question, we injected conditional retrograde AAVrg-hSyn-DIO-mCherry virus into the IL/Pf and anterograde AAV5-CAMKIIa-hChR2-eYFP into the M2/Cg of GlyT2-Cre mice (Figure 5D). We then examined the GlyT2+ cells retrogradely labeled from the thalamus in the PRF and the M2/Cg terminals contacting them. We confirmed the cortical injection sites in M2/Cg (Figure 5E) and their thalamic projection in IL/Pf (Figures 5F and 5G). In the brainstem, we could frequently observe retrogradely labeled PRF/GlyT2+ neurons among the cortical fibers (Figures 5H–5K). Using confocal microscopy, we confirmed M2/Cg terminals formed putative contacts with 82% of all thalamus-projecting PRF/GlyT2+ dendrites ($n = 50$, from 3 mice, Figures 5L–5O). We calculated the mean number of close appositions in a 50- μm -long dendritic segment, which was 2.4 ± 0.22 (Figure 5O).

These data identified cortical inputs on thalamic-projecting PRF/GlyT2+ cells. Together with the data showing that the same layer 5 cell can innervate PRF/GlyT2+ cells and IL/Pf (Figure 4) and PRF/GlyT2+ cell contact IL/Pf (Figure 5)²³ we demonstrated that, in this system cortex, PRF/GlyT2+ cells and thalamus can form multiple nested loops.

(F and G) Merged confocal image of the M2/Cg cortical fibers (green) and PRF/GlyT2+ fibers (magenta) in the thalamus. The red rectangle in (F) indicates the position of the micrograph in (G).

(H) Coronal, stereotactic image of the brainstem. The red rectangle indicates the position of the micrographs in (I)–(K).

(I–K) Confocal micrographs of the anterogradely labeled M2/Cg cortical fibers (green, I), retrogradely labeled thalamus-projecting PRF/GlyT2+ cells (magenta, J), and their merged image (K).

(L–N) High-power confocal microscopic image of the thalamus-projecting PRF/GlyT2+ dendrites (magenta, L) and M2/Cg fibers (magenta, M) and their putative contacts (N, arrowheads).

(O) Percentage of innervated thalamus-projecting PRF/GlyT2+ dendrite (left) and mean number of the close apposition per dendritic segment (right). * $p < 0.05$, ** $p < 0.01$, *** $p < 0.001$; n.s., no significant difference. Source data are provided as a Source Data file. Scale bars, 20 μm (A), 1 mm (E–G), 50 μm (I–K), 5 μm (L–N).

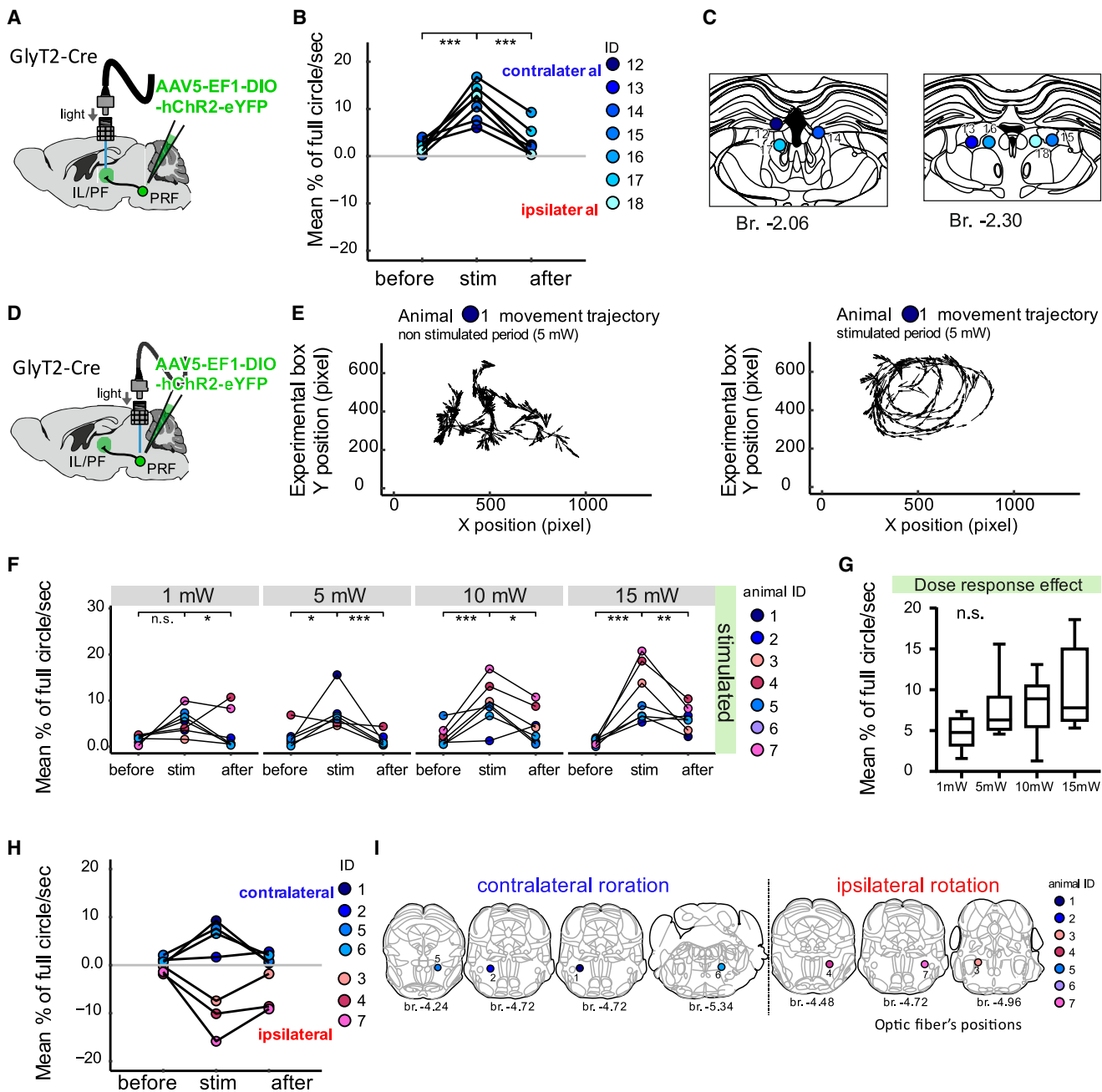


Figure 6. Rotational movements evoked by axonal vs. somatic photoactivation of PRF/GlyT2+ neurons

(A) Experimental design of the photoactivation of thalamus-projecting PRF/GlyT2+ cells via their fibers in the thalamus ($n = 7$ fiber optic fibers).

(B) Contralateral rotations ($n = 7$ fiber optics) displayed as mean rotation angle before, during, and after the stimulus periods following PRF/GlyT2+ fiber stimulation in Pf. The figure represents the average percentage of a full 360° circle per second ($\chi^2 = 10.6, p = 0.005$, Friedman test following Durbin-Conover post hoc, before vs. stim $p < 0.001$; stim vs. after $p < 0.001$).

(C) Schematic view of post hoc identified 7 optic fiber positions for experimental animals in Pf.

(D) Experimental design of the photoactivation of PRF/GlyT2+ somata in the PRF ($n = 7$ fiber optics).

(E) Movement trajectory in one representative mouse displaying contralateral turning (mouse ID: 1). Non-stimulated period (left), stimulated period (right) at 5 mW in the PRF.

(F) Comparison of the absolute values of the mean rotation angle before, during, and after the PRF stimulus periods in the 7 experimental mice (Friedman test following Durbin-Conover post hoc; 1 mW $\chi^2 = 6, p = 0.050$; before vs. stim $p = 0.073$; stim vs. after $p = 0.012$; 5 mW $\chi^2 = 8.33, p = 0.016$; before vs. stim $p = 0.038$; stim vs. after $p < 0.001$; 10 mW $\chi^2 = 10.3, p = 0.006$; before vs. stim $p < 0.001$; stim vs. after $p = 0.014$; 15 mW $\chi^2 = 12.3, p = 0.002$; before vs. stim $p < 0.001$; stim vs. after $p = 0.004$ 5 mW, $\chi^2 = 8.333, p = 0.012$.

(G) Lack of significant dose-response effect on rotation (Friedman test $\chi^2 = 7, p = 0.072$).

(legend continued on next page)

Activation of PRF/GlyT2+ neurons promotes rotational movements

Next, we aimed to examine the behavioral effects of activating the thalamus-projecting PRF/GlyT2+ cells, a key node in the cortex-PRF-thalamus communication. To address this, we injected AAV5-DIO-ChR2-eYFP into the PRF of GlyT2-Cre animals and implanted fiber optics into the thalamus (IL/Pf) ($n = 7$ stimulus site, $n = 2$ animals). We then photoactivated PRF/GlyT2+ fibers unilaterally and bilaterally at various laser intensities (Figure 6A) in IL/Pf. Bilateral stimulation ($n = 20$ stimulation) or unilateral stimulation with higher (15 mW) laser intensities ($n = 24$ stim) resulted in behavior arrest, confirming earlier data.²³ Unilateral stimulation of PRF/GlyT2+ axons in the IL/Pf at lower laser intensity (1, 5, and 10 mW), however, induced rotation always in the contralateral direction (Figure 6B). Rotational movements significantly increased during stimulation and decreased after stimulus termination (Figure 6B; Video S1). Positions of the optic fibers were determined post hoc (Figure 6C).

These findings show that activation of thalamic-projecting PRF/GlyT2+ cells via their axons in IL/Pf consistently leads to contralateral rotation. However, not all PRF/GlyT2+ cells may project to the thalamus. To identify, whether the behavioral effect of activating thalamus-projecting PRF/GlyT2+ cells differ from that of the whole PRF/GlyT2+ population we injected AAV5-DIO-ChR2-eYFP into the PRF in GlyT2-Cre animals and implanted fiber optics, now, into the PRF and photoactivated PRF/GlyT2+ neurons unilaterally via their somata (Figure 6D) at various laser intensities (1, 5, 10, and 15 mW; 5 ms pulse width, 40 Hz for 10 s, $n = 7$ animals).

Since the effect of PRF/GlyT2+ soma activation on movement initiation and maintenance has not been characterized first we measured the traveled distance in the first second of the PRF/GlyT2+ stimulation and the subsequent 9 s (Figure S7A). After the stimulus onset, we found significantly increased movement in the first second of the stimulus relative to the baseline period (before stimulus) with 3 stimulation intensities (1, 10 mW) (Figure S6A). Increased locomotion persisted in the remaining 9 s of the stimulation (Figure S7A). There was no significant dose-response effect with increasing laser light intensity (Figure S7B).

Next, we examined rotational movements during the stimulation of PRF/GlyT2+ somata (10 s) in the same animals (Figure 6E; Videos S2 and S3). Calculated for the whole population ($n = 7$ optic fibers) rotational movements significantly increased compared with the baseline periods upon optogenetic activation at all stimulation intensities (1, 5, 10, and 15 mW, Figure 6F). We found no significant dose-response effect with increasing laser light intensity (Figure 6G). Interestingly, somatic stimulation of PRF/GlyT2+ neurons induced contralateral rotational movements, similar to thalamic stimulation of PRF/GlyT2+ fibers, in only four out of the seven animals. In the remaining three animals ipsilateral rotation was observed (Figure 6H). We found no significant differences in rotational angles between the ipsi- and con-

tralaterally turning animals (ipsilateral vs. contralateral stimulus for all intensity $U = 2$, $p = 0.229$). Post hoc histological identification of optic fiber positions within the PRF revealed no discernible anteroposterior, dorsoventral, or mediolateral differences between the animals exhibiting ipsi- or contralateral rotational movements (Figures 6I, S7C, and S7D).

In the eYFP control animals, the mean traveled distance, and the rotational angle was not significantly different between the baseline and stimulation periods (Figures S7E–S7K; Video S4). Next, we conducted loss-of-function experiments by injecting AAV5-DIO-eNpHR 3.0-eYFP into the PRF ($n = 4$ animals) and implanting optic fibers into the PRF ($n = 8$ optic fibers, Figure S8A). Similar to the gain-of-function experiments (Figures 6 and S7), we found that inhibition of PRF/GlyT2+ somata unilaterally could result in both contra- and ipsiversive rotations (Figure S8C; Video S5). However, for the whole group significant difference in rotational angles was not found (Figures S8C and S8D). Movement initiation was significantly affected only at 15 mW (Figures S8E and S8F).

These findings demonstrate that activation of PRF/GlyT2+ neurons can elicit rotational movements. Activation of thalamic-projecting PRF/GlyT2+ cells via their axons elicits contralateral turning, whereas activation of the entire PRF/GlyT2+ cells population can evoke both ipsi- and contralateral turning.

Distinct projection patterns of thalamus-projecting PRF/GlyT2+ cells

Next, we examined whether the observed differences in turning behavior between PRF/GlyT2+ neurons innervating the thalamus and the entire PRF/GlyT2+ population can be explained by distinct projection patterns (Figure 7). We primarily focused on the gigantocellular nucleus in the medulla (Gi) that has recently been shown to be responsible for the motor commands of turning movements and compared ipsi- and contralateral projections.^{1,10,21}

We investigated the output of thalamus-projecting PRF/GlyT2+ cells by injecting a retrograde Cre-dependent FlpO-containing virus (AAVrg-EF1a-DIO-FlpO) into the IL/Pf thalamus and AAV2/1-EF1a-fDIO-mCherry ($n = 3$) into the PRF in GlyT2-Cre mice. This approach selectively labels the axon arbor of thalamus-projecting PRF/GlyT2+ cells (Figures 7A and S9A–S9H). To label the axons from the entire PRF/GlyT2+ population we injected AAV5-Ef1-DIO-eYFP into PRF of GlyT2-Cre animals ($n = 4$) (Figure 7B).

We found a stark difference in the innervation pattern of Gi between the two approaches. Thalamus-projecting PRF/GlyT2+ cells provided significantly more axons to the ipsilateral Gi (Figure 7A5), whereas labeling the entire PRF/GlyT2+ population resulted in ipsi- and contralateral axons in the Gi of similar density (Figure 7B5). In addition, we found that thalamic-projecting PRF/GlyT2+ cells collateralized primarily in the ipsilateral PRF, whereas we observed substantial

(H) Contralateral ($n = 4$ animals, blueish shades) and ipsilateral ($n = 3$ animals, reddish shades) rotations following PRF/GlyT2 somatic stimulations. The color code of the animals is the same as in (F).

(I) Schematic view of post hoc identified optic fiber position ($n = 7$) in PRF for the 7 experimental mice. Right, fiber optic positions inducing contralateral rotation; left, fiber optic positions inducing ipsilateral rotation. Same notation as in (G). * $p < 0.05$, ** $p < 0.01$, *** $p < 0.001$; n.s., no significant difference. Source data are provided as a Source Data file.

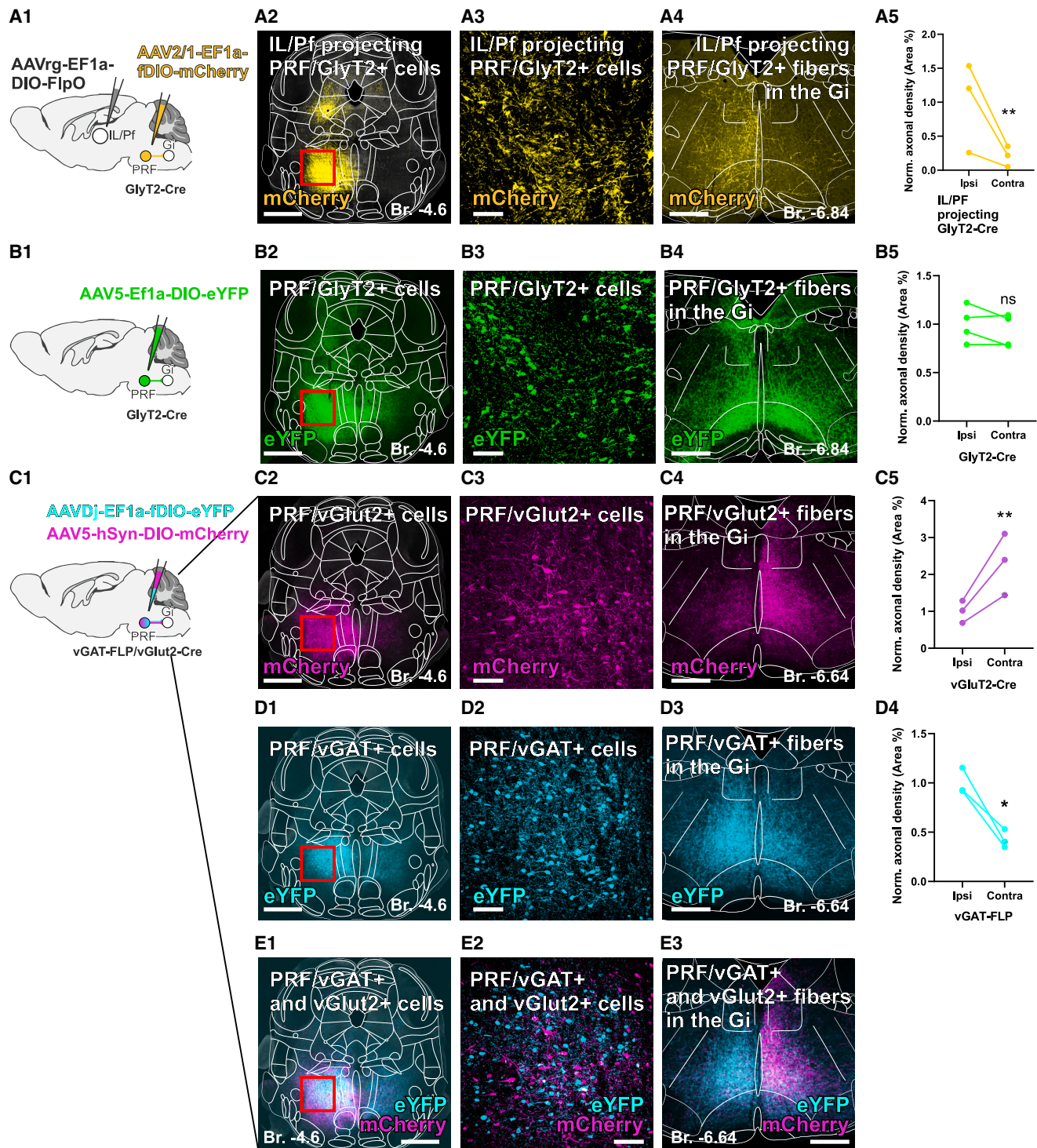


Figure 7. Selective ipsilateral innervation of the gigantocellular nucleus by thalamus-projecting PRF/GlyT2+ cells

(A) (A1) Experimental design to label thalamus-projecting PRF/GlyT2+ cells+ and their axons ($n = 3$ mice). (A2–3) Fluorescent micrograph about virus injection site in the PRF. The red rectangle on (A2) indicates the position of the micrograph in (A3). (A4) Ipsilateral projection of the thalamus-projecting PRF/GlyT2+ cells in the Gi (yellow). (A5) Quantification of ipsilateral and contralateral axonal projections of the thalamus-projecting PRF/GlyT2+ cells in the Gi in GlyT2-Cre mice (paired t test, $t_{(2)} = 22.07$, $p = 0.002$, $n = 3$ mice).

(legend continued on next page)

contralateral projection after labeling the entire PRF/GlyT2+ population (Figures 7A2 and 7B2). The thalamic projections were mainly ipsilateral in both experimental approaches as described before²³ and targeted the dorsolateral sector of Pf (Figure S9H and S9I). In addition, thalamus-projecting PRF/GlyT2+ cells innervated several other regions ipsilaterally including the basal forebrain, hypothalamic regions, and the PAG, which are not known to be involved in turning behavior (Figure S9A–S9G) and are not contacted by thalamus-projecting BG cells.⁹ These data indicate that thalamic-projecting PRF/GlyT2+ cells form a specific subpopulation of the PRF/GlyT2+ cells with a primarily ipsilateral projection pattern that is distinct from the BG outputs.

Recent data have indicated that excitatory, vGLUT2-positive PRF cells project to the contralateral Gi and are responsible for contraversive turning.¹⁰ Our data, here, however, demonstrate that a subpopulation of inhibitory PRF cells mainly project ipsilaterally but still induce contraversive turning. To directly demonstrate the difference between the projection pattern of excitatory and inhibitory PRF population we utilized the fact that glycinergic cells are GABAergic as well^{23,35} and used double transgenic vGAT-Flp/vGlut2-Cre mice to label both the excitatory and the inhibitory projections in the same animals (Figures 7C and S9J). We co-injected AAVDj-EF1a-fDIO-eYFP (cyan) and AAV5-hSyn-DIO-mCherry (magenta) unilaterally into the PRF (Figures 7C–7E) and examined the Gi ($n = 3$). We could confirm that vGlut2+ neurons provide significantly more axons to the contralateral Gi side as described before (Figure 7C), while vGAT+ neurons project bilaterally (Figure 7D), with a significantly higher fiber density on the ipsilateral side.

These experiments together confirm the presence of an inhibitory PRF cell population that projects primarily to the ipsilateral Gi, and activation of these cells can have synergistic behavioral effects with the contralaterally projecting excitatory PRF neurons.

DISCUSSION

Our data show that PRF/GlyT2+ cells are under strong cortical excitatory influence and, in turn, are able to control the spiking activity of thalamic cells in the IL/Pf. We demonstrate a loop-like organization between the cortex, PRF, and the thalamus and show how the output from this loop can influence turning behavior via the thalamus-projecting PRF/GlyT2+ cells.

Multiple nested loops

If two brain centers are connected via a reciprocal loop and in addition there is a third pathway that receives input from one of them and projects to the other, they form nested loops.¹¹ Here, we have shown that, besides the known reciprocal connectivity between M2/Cg and IL/Pf,^{28,29} (1) IL/Pf-projecting M2/Cg cells target PRF/GlyT2+ cells (Figures 4 and S5) and (2) IL/Pf-projecting PRF/GlyT2+ cells are among the targets of M2/Cg neurons (Figure 5). We also show that M2/Cg cells target the same sector in IL/Pf as the thalamus-projecting PRF/GlyT2+ cells. These anatomical data together demonstrate a nested loop organization in the cortex-PRF-thalamus system.

In our functional assays, M2/Cg afferents evoked strong glutamatergic synaptic responses in PRF/GlyT2+ cells both *in vitro* and *in vivo* (Figures 2 and 3). A particular aspect of these experiments was that high-frequency activations of the afferents were followed by faithful synaptic or spiking responses with little depression under both *in vitro* and *in vivo* conditions. In addition, alterations of spontaneous cortical activity were faithfully followed by a change in PRF/GlyT2+ firing patterns. In turn, the activation of the thalamus-projecting PRF/GlyT2+ cells via their axons in the IL/Pf exerted significant inhibitory action on their thalamic targets *in vivo* (Figure 5). Two types of responses were distinguished, a gradual, tonic reduction in firing rate (divisive inhibition) upon repetitive stimulation and the introduction of a brief gap, in the firing activity following each stimulus (phasic inhibition). The inhibited thalamic neurons were consistently found among the PRF/GlyT2+ fibers, providing morphological evidence for a direct inhibitory action. The activity of thalamic cells outside the PRF/GlyT2+ axonal arborization areas remained unaffected by the stimulation. Earlier *in vitro* data demonstrated non-depressing PRF/GlyT2+ IPSCs in IL/Pf cells upon repetitive PRF/GlyT2+ stimulation.²³ This synaptic action may underlie the *in vivo* inhibitory influence observed in this study. In summary, these data indicate that the indirect pathway between M2/Cg and IL/Pf via the PRF/GlyT2+ cells is highly effective and can modify the direct reverberating activity between the cortex and thalamus. The cortex-PRF-thalamus loop is organized according to a similar basic logic to the cortex-BG-thalamus loop. Both systems (1) link interconnected cortical and thalamic stations via an indirect inhibitory loop and (2) receive strong cortical excitation from L5 neurons, which also project to the thalamus. Both BG and PRF provide powerful inhibition to their thalamic targets^{23,36–39} via large axon terminals that establish multiple synapses on a single proximal dendritic

(B) (B1) Experimental design to label all PRF/GlyT2+ cells ($n = 4$ mice). (B2–3) Fluorescent micrograph about virus injection site in PRF. The red rectangle on (B2) indicates the position of the micrograph in (B3). (B4) Bilateral projection of the PRF/GlyT2+ cells in the Gi (green). (B5) Quantification of the ipsilateral vs. contralateral axonal projections from PRF/GlyT2+ cells within the Gi region in GlyT2-Cre mice (paired t test, $t_{(3)} = 1.462$, $p = 0.24$, $n = 4$ mice).

(C) (C1) Scheme of mixed viral injection into PRF in vGAT-Flp/vGlut2-Cre ($n = 3$ mice). (C2–3) Fluorescent micrograph about virus injection site in PRF. The red rectangle on C2 indicates the position of the C3 micrograph. (C4) Bilateral projection with contralateral dominance of PRF/vGlut2+ cells in the Gi (magenta). (C5) Quantification of ipsilateral and contralateral axonal projections from PRF/vGlut2+ cells within the Gi region in vGluT2-Cre/vGAT-FLP mice (paired t test, $t_{(2)} = 19.04$, $p = 0.0027$, $n = 3$ mice).

(D) (D1–2) Fluorescent micrograph about virus injection site in PRF. The red rectangle on (D1) indicates the position of the micrograph in (D2). (D3) Bilateral projection with ipsilateral dominance of PRF/vGAT+ cells in the Gi (cyan). (D4) Quantification of ipsilateral and contralateral axonal projections from PRF/vGAT+ cells within the Gi region in vGluT2-Cre/vGAT-Flp mice (paired t test, $t_{(2)} = 5.61$, $p = 0.0303$, $n = 3$ mice).

(E) (E1–2) Fluorescent micrograph about virus injection site in PRF. The red rectangle on (E1) indicates the position of the micrograph in (E2). (E3) Merged image of PRF/vGAT+ (cyan) and PRF/vGlut2+ (magenta) fibers in the Gi. * $p < 0.05$, ** $p < 0.01$, *** $p < 0.001$; n.s., no significant difference. Source data are provided as a Source Data file. Scale bars, 500 μ m (A2, B2, C2, D1, E1), 100 μ m (A3, B3, C3, D2, E2), 500 μ m (A4, B4, C4, D3, E3).

target in the thalamus.^{23,40} The major difference between the two lies in the complexity of how the cortical input is processed between the input and output stations.

Previous data suggested that linking interconnected thalamic and cortical regions via an extrathalamic inhibitory transfer station, which itself is under strong cortical control, may be a common organizing principle in sensory and motor systems.²⁷ Both the anterior pretectal nucleus and the zona incerta have been shown to be under strong cortical influence and to exert strong inhibition on the somatosensory thalamus, which itself receives powerful excitation from L5 of the primary somatosensory cortex.^{41–43}

Our study demonstrated that most of the M2/Cg L5 pyramidal cells that innervated IL/Pf and PRF/GlyT2+ neurons also provided collaterals to the striatum, the input station of the BG. IL/Pf is the target of both the BG and PRF/GlyT2+ cells.^{23,29} More specifically, a recent study found that PRF-projecting SNR cells innervate the dorsolateral Pf/IL,⁹ the same region targeted by PRF/GlyT2+ cells (this study and Giber et al.²³). This indicates that, despite the fact that the BG and PRF/GlyT2+ cells do not interact directly,¹⁰ they share the same cortical input pattern, and their output is integrated at the same thalamic station, IL/Pf.

Both thalamic-projecting SNR and PRF neurons distribute this message to many other brain centers, but this projection pattern differs significantly. Target-specific retrograde tracings demonstrated that SNR-thalamic neurons mainly target the brainstem center involved in locomotion, orienting responses, and orofacial and muscle tone control.⁹ In contrast, our study shows that the PRF/GlyT2+ cells target brain regions involved in emotional and motivational behavior, arousal, and fear (Figure S8), with the exception of ipsilateral Gi (see below). This suggests that the two loops are likely involved in different behavioral aspects of turning/orienting behavior.

Behavioral effects

Inhibition of IL/Pf cells via the activation of thalamus-projecting PRF/GlyT2+ neurons induced contralateral turning (Figure 6). This effect is consistent with the role of IL/Pf in orienting behavior^{25,26,44} particularly with its role in primarily ipsiversive orientation.²⁴ However, the robust contralateral turning we observed here by activating thalamus-projecting axons in the IL/Pf can be explained by a direct motor effect via inhibition of another brain center. Optogenetic activation of axons are known to propagate antidromically and invade axon collaterals reaching other brain regions.⁴⁵ Examination of the axonal arbor of thalamus-projecting PRF/GlyT2+ cells revealed only one output station known to be involved directly in turning behavior, the Gi (Figures 7 and S9). The presence of these descending collaterals confirmed earlier observations on a PRF-Gi pathway.^{46,47} Our study specifically demonstrated that, while the entire PRF/GlyT2+ cell population projects both to the ipsi- and contralateral Gi equally, the thalamic-projecting subpopulation exhibits a very strong bias toward the ipsilateral Gi. Importantly, it is known that the inhibition of the reticulospinal, Chx10-expressing Gi neurons results in contralateral turning, whereas their activation has opposite effect.^{20,21} Thalamic-projecting PRF/GlyT2+ neurons have a dual, GABAergic, glycinergic phenotype and, as we show here, they can potently inhibit their targets (Figures 5

and S6). Based on these, we propose here that the contralateral turning after the activation of thalamic-projecting PRF/GlyT2+ cells can also arise via the inhibition of ipsilateral Gi through their descending collaterals. This is confirmed by the fact that, during contralateral turning, ipsilateral Gi cells are inhibited and display a strong transient reduction in their activity.¹⁰

Interestingly, based on our results, the contralateral turning induced by activating thalamus-projecting inhibitory PRF/GlyT2+ cells is synergistic with the activation of excitatory PRF/vGLUT2+ cells.¹⁰ In contrast to thalamus-projecting PRF/GlyT2+ cells, PRF/vGLUT2+ cells project to the contralateral Gi. Their activation induces contralateral turning via the activation of contralateral Chx10-expressing neurons (Figure 7).¹⁰ Therefore, based on our proposal activation of PRF can lead to contralateral turning both via a descending, ipsilateral, inhibitory pathway, and a descending, contralateral excitatory pathway to Gi. As our data show, the activation of PRF may arise from the cortex and indeed M2/Cg cortex has already been implicated in orchestrating orienting behavior.^{48–50}

In contrast to photoactivation of thalamus-projecting PRF/GlyT2+ cells contralateral turning could be elicited in only four out of the seven animals following the stimulation of PRF/GlyT2+ cell bodies. In three animals with PRF/GlyT2+ cell body stimulation, ipsilateral, not contralateral rotation occurred suggesting a different neuronal mechanism. Importantly, we did not find systematic differences in the localization of the optic fibers inducing either ipsi- or contralateral rotation. In parallel with these behavioral data, when we labeled the descending axons of the entire PRF/GlyT2+ cell population to Gi we found no difference between the innervation of ipsi- and contralateral sides. In contrast, there was a very strong ipsilateral bias when we were labeling the thalamus-projecting PRF/GlyT2+ cells (see above). This suggests the existence of a sizable non-thalamus-projecting PRF/GlyT2+ cell population that innervates the contralateral side rather than the ipsilateral side. Activating these cells would inhibit contralateral Gi, obviously leading to ipsilateral turning. Thus, our data suggest that circuit elements responsible for ipsi- or contralateral rotation in the PRF are intermingled. These results align well with recent discoveries demonstrating the modularity or granularity of basal ganglia and brainstem motor networks.² According to these findings, neuronal populations with specialized functions in the brainstem can be located in close proximity and still coordinate different types of motor program. Along these lines, it has been shown previously that, in the PRF, stimulation sites including unilateral or bilateral atonia via the spinal cord are mixed in the PRF,¹⁹ indicating that granularity² may also apply to this region.

Limitations of the study

Our study leaves several questions open for future investigations. First, many cortical inputs were not in close apposition to PRF/GlyT2+ cells, suggesting that the PRF/vGLUT2+ neurons might also be contacted. However, the direct synaptic input and action of cortex on vGLUT2+ neurons remain to be established. Second, in parallel with inhibitory PRF cells, vGLUT2+ PRF cells also provided input to the same sector of IL/Pf (Figure S9). The role of this “push-pull” projection from PRF to the thalamus requires further investigation. Third, in contrast to the

PRF/GlyT2+ labeling that highlighted similar innervation of both sides of Gi equally, tracing PRF/vGAT+ cells revealed a strong ipsilateral bias in Gi (Figure 7D). Since all GlyT2+ cells are vGAT+ as well,²³ this finding suggests the presence of a sizable vGAT+/GlyT2-cell population in the PRF that provides strong ipsilateral inhibition and thus can participate in contralateral turning. Finally, our data do not unequivocally demonstrate whether the ascending and/or the descending collaterals of thalamus-projecting PRF/GlyT2+ cells participate in the observed turning/orienting behaviors. Based on the earlier data, inhibition of both the Pf and the Gi can lead to contralateral bias^{20,21,24}; thus, in principle, both the PRF-thalamic and PRF-Gi collaterals can synergistically command various aspects of the turning/orienting behavior. However, clarification of this question certainly needs to be addressed by future studies.

Conclusions

Our data show that cortical messages arising from higher-order motor cortices can be processed parallelly by two distinct cortico-subcortical loops: the cortex-BG-thalamus and the cortex-PRF-thalamus loops. Apart from the thalamus, the two loops target distinct regions/cell types in the brainstem. Still, our data indicate that cortical action on PRF and the BG can synergistically affect turning behavior via differential action on ipsi- vs. contralateral reticulospinal neurons in Gi.

RESOURCE AVAILABILITY

Lead contact

Further information and requests for resources and reagents should be directed to and will be fulfilled by the lead contact, László Acsády (acsady@koki.hu).

Materials availability

This study did not generate new unique reagents.

Data and code availability

Source data have been deposited at Zenodo and are publicly available as of the date of publication. Accession numbers are listed in the key resources table.

- Data: source data are deposited in Zenodo, <https://doi.org/10.5281/zenodo.14500202>.
- Code: source code are deposited in Zenodo and available in Github, https://github.com/viktorpm/glyci_analysis, <https://doi.org/10.5281/zenodo.14500202>.
- All other items: all relevant data supporting the findings of this study are available within the article and its supplementary materials.

ACKNOWLEDGMENTS

We thank the Light Microscopy Center, the Electron Microscopy Center, and the Virus Technology Unit at the Institute of Experimental Medicine for providing support for the experiments. The authors would like to thank Krisztina Faddi for their excellent technical assistance, Gábor Nyíri for providing the AAVrg-EF1a-DIO-FlpO-WPRE-HGHPA AAVrg-EF1a-Cre and AAVrg-hSyn-DIO-mCherry virus constructs, and Csaba Dávid for his help in quantifying the cortical input density in PRF. This research was funded by an ERC Advanced Grant FRONTHAL, 742595 (to L.A.); the European Union project within the framework of the Artificial Intelligence National Laboratory RRF-2.3.1-21-2022-00004 (to L.A.); and the Hungarian Academy of Sciences – “Lendület” Program LP2023-2/2023 (to L.A.). This research work was conducted with the support of the National Academy of Scientist Education Pro-

gram of the National Biomedical Foundation under the sponsorship of the Hungarian Ministry of Culture and Innovation.

AUTHOR CONTRIBUTIONS

Conceptualization, E.B., V.M.P., L.B., and L.A.; methodology, E.B., V.M.P., M.A.D., L.B., K.K., and L.A.; software, V.M.P., E.B., and L.A.; validation, E.B., V.M.P., L.B., and L.A.; formal analysis, E.B., V.M.P., and L.B.; investigation, E.B., V.M.P., M.A.D., L.B., and K.K.; resources, L.A. and M.A.D.; visualization, E.B., V.P., and L.B.; funding acquisition, M.A.D. and L.A.; project administration, L.A.; supervision, L.A.; writing – original draft, E.B., M.A.D., V.M.P., L.B., and L.A.; writing – review & editing, E.B., L.B., V.M.P., and L.A.

DECLARATION OF INTERESTS

The authors declare no competing interests.

STAR METHODS

Detailed methods are provided in the online version of this paper and include the following:

- KEY RESOURCES TABLE
- EXPERIMENTAL MODEL AND STUDY PARTICIPANT DETAILS
 - Animal housing
- METHOD DETAILS
 - Surgeries
 - Histology
 - In vivo electrophysiology
 - Behavior
- QUANTIFICATION AND STATISTICAL ANALYSIS
 - Axonal density analysis
 - Density mapping analysis
 - In vitro analysis
 - Analysis for juxtacellular recordings
 - PFC photoactivation
 - Spontaneous frontal cortical activity changes
 - Thalamocortical neuronal activity
 - Video analysis for behavior
 - Statistics

SUPPLEMENTAL INFORMATION

Supplemental information can be found online at <https://doi.org/10.1101/j.celrep.2025.115230>.

Received: August 30, 2024

Revised: September 13, 2024

Accepted: January 2, 2025

Published: January 22, 2025

REFERENCES

1. Leiras, R., Clegg, J.M., and Kiehn, O. (2022). Brainstem Circuits for Locomotion. *Annu. Rev. Neurosci.* 45, 63–85. <https://doi.org/10.1146/ANNUREV-NEURO-082321-025137>.
2. Arber, S., and Costa, R.M. (2022). Networking brainstem and basal ganglia circuits for movement. *Nat. Rev. Neurosci.* 23, 342–360. <https://doi.org/10.1038/s41583-022-00581-w>.
3. Smith, Y., Raju, D.V., Pare, J.F., and Sidibe, M. (2004). The thalamostriatal system: A highly specific network of the basal ganglia circuitry. *Trends Neurosci.* 27, 520–527. <https://doi.org/10.1016/j.tins.2004.07.004>.
4. Cui, G., Jun, S.B., Jin, X., Pham, M.D., Vogel, S.S., Lovinger, D.M., and Costa, R.M. (2013). Concurrent activation of striatal direct and indirect pathways during action initiation. *Nature* 494, 238–242. <https://doi.org/10.1038/nature11846>.

5. Díaz-Hernández, E., Contreras-López, R., Sánchez-Fuentes, A., Rodríguez-Sibrán, L., Ramírez-Jarquín, J.O., and Tecuapetla, F. (2018). The Thalamostriatal Projections Contribute to the Initiation and Execution of a Sequence of Movements. *Neuron* 100, 739–752.e5. <https://doi.org/10.1016/j.neuron.2018.09.052>.
6. Foster, N.N., Barry, J., Korobkova, L., Garcia, L., Gao, L., Becerra, M., Sherafat, Y., Peng, B., Li, X., Choi, J.H., et al. (2021). The mouse cortico–basal ganglia–thalamic network. *Nature* 598, 188–194. <https://doi.org/10.1038/S41586-021-03993-3>.
7. Hintiryan, H., Foster, N.N., Bowman, I., Bay, M., Song, M.Y., Gou, L., Yamashita, S., Bienkowski, M.S., Zingg, B., Zhu, M., et al. (2016). The mouse cortico–striatal projectome. *Nat. Neurosci.* 19, 1100–1114. <https://doi.org/10.1038/nn.4332>.
8. Alexander, G.E., DeLong, M.R., and Strick, P.L. (1986). Parallel Organization of Functionally Segregated Circuits Linking Basal Ganglia and Cortex. *Annu. Rev. Neurosci.* 9, 357–381. <https://doi.org/10.1146/ANNREV.NE.09.030186.002041>.
9. McElvain, L.E., Chen, Y., Moore, J.D., Brigidi, G.S., Bloodgood, B.L., Lim, B.K., Costa, R.M., and Kleinfeld, D. (2021). Specific populations of basal ganglia output neurons target distinct brain stem areas while collateralizing throughout the diencephalon. *Neuron* 109, 1721–1738.e4. <https://doi.org/10.1016/J.NEURON.2021.03.017>.
10. Cregg, J.M., Sidhu, S.K., Leiras, R., and Kiehn, O. (2024). Basal ganglia–spinal cord pathway that commands locomotor gait asymmetries in mice. *Nat. Neurosci.* 27, 716–727. <https://doi.org/10.1038/s41593-024-01569-8>.
11. Acsády, L. (2023). Heterogeneity of Thalamic Input Landscapes. In *The Cerebral Cortex and Thalamus*, W.M. Usrey and S.M. Sherman, eds., pp. 32–44. <https://doi.org/10.1093/MED/9780197676158.003.0004>.
12. Jaramillo, J., and Guo, Z.V. (2023). Thalamocortical Contributions to Neural Dynamics and Behavior. In *The Cerebral Cortex and Thalamus*, W.M. Usrey and S.M. Sherman, eds., pp. 367–380. <https://doi.org/10.1093/MED/9780197676158.003.0035>.
13. McNaughton, N., and Vann, S.D. (2022). Construction of complex memories via parallel distributed cortical–subcortical iterative integration. *Trends Neurosci.* 45, 550–562. <https://doi.org/10.1016/J.TINS.2022.04.006>.
14. Berendse, H.W., and Groenewegen, H.J. (1990). Organization of the thalamostriatal projections in the rat, with special emphasis on the ventral striatum. *J. Comp. Neurol.* 299, 187–228. <https://doi.org/10.1002/CNE.902990206>.
15. Pare, D., and Smith, Y. (1996). Thalamic Collaterals of Corticostriatal Axons: Their Termination Field and Synaptic Targets in Cats. *J. Comp. Neurol.* 372, 551. [https://doi.org/10.1002/\(SICI\)1096-9861\(19960902\)372:4](https://doi.org/10.1002/(SICI)1096-9861(19960902)372:4).
16. Levesque, M., Gagnon, S., and Parent, A.; Deschenes (1996). Axonal arborizations of corticostriatal and corticothalamic fibers arising from the second somatosensory area in the rat. *Cereb Cortex* 6, 759–770.
17. Economo, M.N., Viswanathan, S., Tasic, B., Bas, E., Winnubst, J., Menon, V., Graybuck, L.T., Nguyen, T.N., Smith, K.A., Yao, Z., et al. (2018). Distinct descending motor cortex pathways and their roles in movement. *Nature* 563, 79–84. <https://doi.org/10.1038/s41586-018-0642-9>.
18. Mileykovskiy, B.Y., Kiyashchenko, L.I., Kodama, T., Lai, Y.Y., and Siegel, J.M. (2000). Activation of Pontine and Medullary Motor Inhibitory Regions Reduces Discharge in Neurons Located in the Locus Coeruleus and the Anatomical Equivalent of the Midbrain Locomotor Region. *J. Neurosci.* 20, 8551–8558. <https://doi.org/10.1523/JNEUROSCI.20-22-08551.2000>.
19. Hajnik, T., Lai, Y.Y., and Siegel, J.M. (2000). Atonia-Related Regions in the Rodent Pons and Medulla. *J. Neurophysiol.* 84, 1942–1948. <https://doi.org/10.1152/JN.2000.84.4.1942>.
20. Goñi-Erro, H., Selvan, R., Caggiano, V., Leiras, R., and Kiehn, O. (2023). Pedunculopontine Chx10+ neurons control global motor arrest in mice. *Nat. Neurosci.* 2023, 1–13. <https://doi.org/10.1038/s41593-023-01396-3>.
21. Cregg, J.M., Leiras, R., Montalant, A., Wanken, P., Wickersham, I.R., and Kiehn, O. (2020). Brainstem neurons that command mammalian locomotor asymmetries. *Nat. Neurosci.* 23, 730–740. <https://doi.org/10.1038/S41593-020-0633-7>.
22. Zeilhofer, H.U., Studler, B., Arabadzisz, D., Schweizer, C., Ahmadi, S., Layh, B., Bösl, M.R., and Fritschy, J.M. (2005). Glycinergic neurons expressing enhanced green fluorescent protein in bacterial artificial chromosome transgenic mice. *J. Comp. Neurol.* 482, 123–141. <https://doi.org/10.1002/CNE.20349>.
23. Giber, K., Diana, M.A., Plattner, V., Dugué, G.P., Bokor, H., Rousseau, C.V., Maglóczky, Z., Havas, L., Hangya, B., Wildner, H., et al. (2015). A subcortical inhibitory signal for behavioral arrest in the thalamus. *Nat. Neurosci.* 18, 562–568. <https://doi.org/10.1038/nn.3951>.
24. Fallon, I.P., Hughes, R.N., Severino, F.P.U., Kim, N., Lawry, C.M., Watson, G.D.R., Roshchina, M., and Yin, H.H. (2023). The role of the parafascicular thalamic nucleus in action initiation and steering. *Curr. Biol.* 33, 2941–2951.e4. <https://doi.org/10.1016/j.cub.2023.06.025>.
25. Matsumoto, N., Minamimoto, T., Graybiel, A.M., and Kimura, M. (2001). Neurons in the thalamic CM-Pf complex supply striatal neurons with information about behaviorally significant sensory events. *J. Neurophysiol.* 85, 960–976. <https://doi.org/10.1152/jn.2001.85.2.960>.
26. Minamimoto, T., and Kimura, M. (2002). Participation of the thalamic CM-Pf complex in attentional orienting. *J. Neurophysiol.* 87, 3090–3101. <https://doi.org/10.1152/JN.2002.87.6.3090>.
27. Halassa, M.M., and Acsády, L. (2016). Thalamic Inhibition: Diverse Sources, Diverse Scales. *Trends Neurosci.* 39, 680–693. <https://doi.org/10.1016/j.tins.2016.08.001>.
28. Gonzalo-Martín, E., Alonso-Martínez, C., Sepúlveda, L.P., and Clasca, F. (2023). Micropopulation mapping of the mouse parafascicular nucleus connections reveals diverse input–output motifs. *Front. Neuroanat.* 17, 1305500. [https://doi.org/10.1016/s0165-0173\(02\)00181-9](https://doi.org/10.1016/s0165-0173(02)00181-9).
29. Van der Werf, Y.D., Witter, M.P., and Groenewegen, H.J. (2002). The intralaminar and midline nuclei of the thalamus. Anatomical and functional evidence for participation in processes of arousal and awareness. *Brain Res. Brain Res. Rev.* 39, 107–140.
30. Harris, J.A., Mihalas, S., Hirokawa, K.E., Whitesell, J.D., Choi, H., Bernard, A., Bohn, P., Caldejon, S., Casal, L., Cho, A., et al. (2019). Hierarchical organization of cortical and thalamic connectivity. *Nature* 575, 195–202. <https://doi.org/10.1038/S41586-019-1716-Z>.
31. Pinault, D. (1996). A novel single-cell staining procedure performed in vivo under electrophysiological control: Morpho-functional features of juxtacellularly labeled thalamic cells and other central neurons with biocytin or Neurobiotin. *J. Neurosci. Methods* 65, 113–136. [https://doi.org/10.1016/0160-0270\(95\)00144-1](https://doi.org/10.1016/0160-0270(95)00144-1).
32. Groh, A., Bokor, H., Mease, R.A., Plattner, V.M., Hangya, B., Stroh, A., Deschenes, M., and Acsády, L. (2014). Convergence of cortical and sensory driver inputs on single thalamocortical cells. *Cereb. Cortex* 24, 3167–3179. <https://doi.org/10.1093/CERCOR/BHT173>.
33. Economo, M.N., Clack, N.G., Lavis, L.D., Gerfen, C.R., Svoboda, K., Myers, E.W., and Chandrashekhar, J. (2016). A platform for brain-wide imaging and reconstruction of individual neurons. *Elife* 5, e10566. <https://doi.org/10.7554/ELIFE.10566>.
34. Arnts, H., Coolen, S.E., Fernandes, F.W., Schuurman, R., Krauss, J.K., Groenewegen, H.J., Van Den Munckhof, P., and Arnts, H. (2023). The intralaminar thalamus: a review of its role as a target in functional neurosurgery. *Brain Commun.* 5, fcad003. <https://doi.org/10.1093/BRAINCOMMS/FCAD003>.
35. Jonas, P., Bischofberger, J., and Sandkühler, J. (1998). Corelease of two fast neurotransmitters at a central synapse. *Science* 281, 419–424. <https://doi.org/10.1126/science.281.5375.419>.
36. Ueki, A. (1983). The mode of nigro-thalamic transmission investigated with intracellular recording in the cat. *Exp. Brain Res.* 49, 116–124.

37. Chevalier, G., and Deniau, J.M. (1982). Inhibitory nigral influence on cerebellar evoked responses in the rat ventromedial thalamic nucleus. *Exp. Brain Res.* 48, 369–376. <https://doi.org/10.1007/BF00238613>.
38. Goldberg, J.H., Farries, M.A., and Fee, M.S. (2013). Basal ganglia output to the thalamus: still a paradox. *Trends Neurosci.* 36, 695–705. <https://doi.org/10.1016/J.TINS.2013.09.001>.
39. Anderson, M.E., Postupna, N., and Ruffo, M. (2003). Effects of high-frequency stimulation in the internal globus pallidus on the activity of thalamic neurons in the awake monkey. *J. Neurophysiol.* 89, 1150–1160. <https://doi.org/10.1152/jn.00475.2002>.
40. Bodor, Á.L., Giber, K., Rovó, Z., Ulbert, I., and Acsády, L. (2008). Structural correlates of efficient GABAergic transmission in the basal ganglia-thalamus pathway. *J. Neurosci.* 28, 3090–3102. <https://doi.org/10.1523/JNEUROSCI.5266-07.2008>.
41. Barthó, P., Freund, T.F., and Acsády, L. (2002). Selective GABAergic innervation of thalamic nuclei from zona incerta. *Eur. J. Neurosci.* 16, 999–1014.
42. Barthó, P., Slézia, A., Varga, V., Bokor, H., Pinault, D., Buzsáki, G., and Acsády, L. (2007). Cortical Control of Zona Incerta. *J. Neurosci.* 27, 1670–1681. <https://doi.org/10.1523/JNEUROSCI.3768-06.2007>.
43. Bokor, H., Frère, S.G.A., Eyre, M.D., Slézia, A., Ulbert, I., Lüthi, A., and Acsády, L. (2005). Selective GABAergic control of higher-order thalamic relays. *Neuron* 45, 929–940.
44. Kinomura, S., Larsson, J., Gulyás, B., and Roland, P.E. (1996). Activation by Attention of the Human Reticular Formation and Thalamic Intralaminar Nuclei. *Science* 271, 512–515. <https://doi.org/10.1126/SCIENCE.271.5248.512>.
45. Mátyás, F., Komlósi, G., Babiczky, Á., Kocsis, K., Barthó, P., Barsy, B., Dávid, C., Kanti, V., Porrero, C., Magyar, A., et al. (2018). A highly collateralized thalamic cell type with arousal-predicting activity serves as a key hub for graded state transitions in the forebrain. *Nat. Neurosci.* 21, 1551–1562. <https://doi.org/10.1038/s41593-018-0251-9>.
46. Gallager, D.W., and Pert, A. (1978). Afferents to brain stem nuclei (brain stem raphe, nucleus reticularis pontis caudalis and nucleus gigantocellularis) in the rat as demonstrated by microiontophoretically applied horseradish peroxidase. *Brain Res.* 144, 257–275. [https://doi.org/10.1016/0006-8993\(78\)90153-1](https://doi.org/10.1016/0006-8993(78)90153-1).
47. Hermann, D.M., Luppi, P.H., Peyron, C., Hinckel, P., and Jouvet, M. (1997). Afferent projections to the rat nuclei raphe magnus, raphe pallidus and reticularis gigantocellularis pars α demonstrated by iontophoretic application of cholera toxin (subunit b). *J. Chem. Neuroanat.* 13, 1–21. [https://doi.org/10.1016/S0891-0618\(97\)00019-7](https://doi.org/10.1016/S0891-0618(97)00019-7).
48. Erlich, J.C., Bialek, M., and Brody, C.D. (2011). A cortical substrate for memory-guided orienting in the rat. *Neuron* 72, 330–343. <https://doi.org/10.1016/j.neuron.2011.07.010>.
49. Hanks, T.D., Kopec, C.D., Brunton, B.W., Duan, C.A., Erlich, J.C., and Brody, C.D. (2015). Distinct relationships of parietal and prefrontal cortices to evidence accumulation. *Nature* 520, 220–223. <https://doi.org/10.1038/nature14066>.
50. Brecht, M. (2011). Movement, Confusion, and Orienting in Frontal Cortices. *Neuron* 72, 193–196. <https://doi.org/10.1016/J.NEURON.2011.10.002>.
51. Schindelin, J., Arganda-Carreras, I., Frise, E., Kaynig, V., Longair, M., Pietzsch, T., Preibisch, S., Rueden, C., Saalfeld, S., Schmid, B., et al. (2012). Fiji: an open-source platform for biological-image analysis. *Nat. Methods* 9, 676–682. <https://doi.org/10.1038/nmeth.2019>.

STAR★METHODS

KEY RESOURCES TABLE

REAGENT or RESOURCE	SOURCE	IDENTIFIER
Antibodies		
Rabbit Anti-mCherry Polyclonal Antibody, Unconjugated	BioVision	Cat# 5993-100, RRID:AB_1975001
Chicken anti-eGFP Polyclonal Antibody	Thermo Fisher Scientific	Cat# A10262, RRID:AB_2534023)
ImmPRESS-AP Anti-Rabbit Ig Reagent	Vector Laboratories	Cat# MP-5401, RRID:AB_2336536
Cy3-AffiniPure Fab Fragment Goat Anti-Rabbit IgG (H + L)	Jackson ImmunoResearch Labs	Cat# 111-167-003, RRID:AB_2313593)
Cy3-AffiniPure Donkey Anti-Rabbit IgG (H + L)	Jackson ImmunoResearch Labs	Cat# 711-165-152, RRID:AB_2307443
Goat anti-Chicken IgY (H + L) Secondary Antibody, Alexa Fluor TM 488	Thermo Fisher Scientific	Cat# A-11039, RRID:AB_2534096
Alexa Fluor 488 AffiniPure Donkey Anti-Chicken IgY (IgG) (H + L)	Jackson ImmunoResearch Labs	Cat# 703-545-155, RRID:AB_2340375)
Cy3-Streptavidin antibody	Jackson ImmunoResearch Labs	Cat# 016-160-084, RRID:AB_2337244)
Bacterial and virus strains		
AAV5.EF1.dflox.hChR2(H134R)-mCherry.WPRE.hGH	UNC Vector Core	Based on Addgene plasmid RRID:Addgene_20297
AAVrg-EF1a-DIO-FlpO-WPRE-HGHpA	Addgene	RRID:Addgene_87306
AAV2/1-EF1a-fDIO-mCherry	Addgene	RRID:Addgene_114471
AAVrg-EF1a-Cre	Addgene	RRID:Addgene_55636
AAV5.EF1.dflox.hChR2(H134R)-mCherry.WPRE.hGH	UNC Vector Core	Based on Addgene plasmid RRID:Addgene_20297
AAV5-CAMKIIa-CHR2(H134R)-EYFP	Addgene	RRID:Addgene_26969
AAVrg-hSyn-DIO-mCherry	Addgene	RRID:Addgene_50459
AAV5.EF1a.DIO.hChR2(H134R)-eYFP.WPRE.hGH	UNC Vector Core	Based on Addgene plasmid RRID:Addgene_20298
AAV5-Ef1a-DIO eNpHR 3.0-EYFP	Addgene	RRID:Addgene_26966
AAV5.EF1a.DIO.eYFP.WPRE.hGH	Penn Core	Based on Addgene plasmid RRID:Addgene_27056
AAV1-EF1a-fDIO-EYFP	Addgene	RRID:Addgene_55641
AAV5-hSyn-DIO-mCherry	Addgene	RRID:Addgene_50459
AAVDJ-EF1a-fDIO-EYFP-WPRE	UNC Vector Core	Based on Addgene plasmid RRID:Addgene_55641
Chemicals, peptides, and recombinant proteins		
3,3'-Diaminobenzidine tetrahydrochloride	Sigma-Aldrich	Cat# D5905
VECTASTAIN [®] ABC-HRP Kit, Peroxidase (Standard)	Vector Laboratories	Cat# PK-4000
Durcupan ACM	Sigma-Aldrich	Cat# 44610
'Dil'; DilC18(3)	ThermoFisher Scientific	Cat# D282
CsMeSO ₃	Sigma-Aldrich	Cat# C1426
TEA-Cl	Sigma-Aldrich	Cat# T2265
4-AP	Sigma-Aldrich	Cat# A1910
K2-creatine phosphate	Sigma-Aldrich	Cat# 237911

(Continued on next page)

Continued

REAGENT or RESOURCE	SOURCE	IDENTIFIER
Deposited data		
Simple Mouse Tracker	joseaccruz	https://github.com/joseaccruz/SimpleMouseTracker
Code: Glyci analysis – R code for the paper	This paper	https://github.com/viktorpm/glyci_analysis https://doi.org/10.5281/zendodo.14500202
Source data	This paper	in Zenodo, https://doi.org/10.5281/zendodo.14500202
Experimental models: Organisms/strains		
Mus musculus: GlyT2-Cre (Tg) - B6129F1	The Jackson Laboratory	RRID:IMSR_JAX:038514
Mus musculus: C57BL/6J	The Jackson Laboratory	RRID:IMSR_JAX:000664
Mus musculus: BAC_glyt2/GFP -C57Bl/6J29	The Jackson Laboratory	RRID:IMSR_JAX:038516
Mus musculus: vglut2/cre	The Jackson Laboratory	RRID:IMSR_JAX:016963
Mus musculus: vGAT/t2A-Flpo	The Jackson Laboratory	RRID:IMSR_JAX:029591
Mus musculus: Rbp4/cre//BAC_glyt2/GFP (TgTg) - C57Bl/6J	This paper	N/A
Mus musculus: vGAT/t2A-Flpo//BAC-vglut2/cre (TmTg)-C57Bl/6J	This paper	N/A
Software and algorithms		
FIJI	Schindelin et al. ⁵¹	N/A
Jamovi v 2.328	The jamovi project (2022). jamovi. (Version 2.3) [Computer Software]. Retrieved from https://www.jamovi.org .	N/A
Prism 8 software (GraphPad)	https://www.graphpad.com/features	N/A
Adobe Photoshop	https://www.adobe.com/products/photoshop.html	N/A
Corel Draw	https://www.coreldraw.com/en/	N/A
R Foundation for Statistical Computing, Vienna, Austria.	https://www.R-project.org/	N/A
Adobe Premiere Pro	https://www.adobe.com/products/premiere.html	N/A

EXPERIMENTAL MODEL AND STUDY PARTICIPANT DETAILS

Animal housing

All experimental procedures were approved by the Institutional Ethical Codex, Hungarian Act of Animal Care and Experimentation (1998, XXVIII, section 243/1998) and the Institutional Animal Care and Use Committee of the Institute of Experimental Medicine, Hungarian Research Network, Budapest and by the regulations of the European Union guidelines (directive 2010/63/EU). The experiments were performed by the National Animal Research Authorities of Hungary (PE/EA/877-7/2020). We used healthy, adult male mice (40–150 days) for the experiments. We used the following mice strains: GlyT2-Cre (Tg) - B6129F1 and Bl6Fx, Rbp4/cre//BAC_glyt2/GFP (TgTg) - C57Bl/6J, vGAT/t2A-Flpo//BAC-vglut2/cre (TmTg)-C57Bl/6J, BAC_glyt2/GFP -C57Bl/6J.^{22,23} Mice were entrained in a 12-h light/dark cycle with food and water available as *ad libitum*. We performed animal research according to the 3R principles.

METHOD DETAILS

Surgeries

Anesthesia

The surgeries were done for all experiments (anatomy, electrophysiology, optogenetics) based on the following protocol. As anesthetics, mice received an intraperitoneal injection of ketamine (111 mg/kg, Produlab Pharma, #07/01/2302) and xylazine (4.3 mg/kg, Produlab Pharma, #07/03/2303). For the maintenance of the anesthesia, intramuscular injection of ketamine/xylazine was given every 30–50 min during the experiments. The head of the animal was fixed in a stereotaxic apparatus (David Kopf Instruments,

Tujunga, California 91042, Model 900 Small Animal Stereotaxic Instrument). In one experimental condition, we used urethane anesthesia during IL/Pf *in vivo* juxtacellular recordings (0.12–0.15 g/100 g).

Virus injections and fiber optics implantations

For the anatomical investigations and *in vitro* and *in vivo* electrophysiological experiments, all stereotaxic tracer injections were performed using a glass pipette (intraMARK, 20–30- μ m tip diameter, BLAUBRAND, injection flow: 25 nL/min) connected to a syringe and a stereotaxic micromanipulator (Kopf Instruments). After injection, the capillary was left at the injection site for 5–10 min before slow withdrawal to allow diffusion and minimize backflow. The mice were perfused or were used for experiments following a 3–6-week survival time.

For the investigation of the cortico L5-PRF pathway, we used Rbp4/cre//BAC_glyt2/GFP (TgTg) mouse line (altogether $n = 25$ mice) ($n = 11$ for the anatomical investigation, $n = 7$ for *in vitro* electrophysiology and $n = 7$ for *in vivo* electrophysiology).

For all (*in vivo* and *in vitro*) electrophysiology and nine of the anatomical experiments the following virus injection design was used. We injected AAV5.EF1.d flox.hChR2(H134R)-mCherry.WPRE.hGH (based on Addgene plasmid RRID:Addgene_20297, UNC Vector Core) cre-dependent virus into the frontal cortex, M2/Cg (AP: Br.1 mm and 2 mm; ML: Br.0.5 mm; DV: 0.7 mm; bilaterally into 2-2 AP position, 80 nL each, 4 injection/mouse). For *in vivo* electrophysiology L5 photoactivation, the optic fibers (100 μ m, 0.22 NA) were positioned above the virus injection site (M2/Cg).

For labeling the axon collaterals of PF targeting L5 neurons we used two types of virus injection design ($n = 4$), where in two cases we injected AAVrg-EF1a-DIO-FloP-WPRE-HGHPa (RRID:Addgene_87306) virus into the Pf unilaterally (AP: -2, ML: 0.5, DV: 3; 30 nL). After three weeks we injected AAV2/1-EF1a-fDIO-mCherry (RRID:Addgene_114471) virus into the M2/Cg (AP: Br.1 mm and 2 mm; ML: Br.0.5 mm; DV: 0.7 mm; unilaterally into 2 AP position, 80 nL each, 2 injection/mouse).

The other two cases we used BAC_glyt2/gfp mouse line ($n = 2$) and we injected AAvg-EF1a-Cre (RRID:Addgene_55636) into the Pf unilaterally (AP: -2, ML: 0.5, DV: 3; 30 nL). We waited three weeks and injected AAV5.EF1.d flox.hChR2(H134R)-mCherry.WPRE.hGH (based on Addgene plasmid RRID:Addgene_20297, UNC Vector Core) into the M2 (AP: Br.1 mm and 2 mm; ML: Br.0.5 mm; DV: 0.7 mm; unilaterally into 2 AP position, 80 nL each, 2 injection/mouse).

The last experimental design of the cortico L5-PRF pathway's investigation was labeling M2 axons on Pf-projecting PRF/GlyT₊ neurons in GlyT2-Cre mice ($n = 4$). We injected AAV5-CAMKIIa-CHR2(H134R)-EYFP (RRID:Addgene_26969) into the M2 (AP: Br.1 mm and 2 mm; ML: Br.0.5 mm; DV: 0.7 mm; unilaterally into 2 AP position, 80 nL each, 2 injection/mouse) and AAvg-hSyn-DIO-mCherry (RRID:Addgene_50459) into Pf unilaterally (AP: -2, ML: 0.5, DV: 3; 30 nL).

For the investigation of the PRF/GlyT2+-thalamic pathways altogether $n = 32$ adult GlyT2-Cre male mice were used including the *in vivo* optogenetic behavioral ($n = 17$), electrophysiology (juxtacellular recording, $n = 13$) experiments and anatomical investigation ($n = 3$). For optogenetic activation of PRF/GlyT2+ cells, we injected AAV5.EF1a.DIO.hChR2(H134R)-eYFP.WPRE.hGH (based on Addgene plasmid RRID:Addgene_20298, UNC Vector Core). For optogenetic activation of PRF/GlyT2+ fibers in the IL/Pf we did the same injections but bilaterally. For optogenetic inhibition of the PRF/GlyT2+ somata, we injected AAV5-Ef1a-DIO.eNpHR 3.0-EYFP (RRID:Addgene_26966) into PRF bilaterally (AP:-4.4, ML:0.8, DV: 4.2, 100–100 nL). In the control experiment we injected AAV5.EF1a.DIO.eYFP.WPRE.hGH (based on Addgene plasmid RRID:Addgene_27056, Penn Core) virus into the PRF unilaterally (AP:-4.4, ML:0.8, DV: 4.2, 100 nL).

After virus injection the optic fibers (Thorlabs, FG105UCA, Ø105 μ m core, 0.22 NA) were implanted into the PRF ($n = 15$ optic fiber in $n = 11$ mice, AP:-4.4, ML:0.8, DV: 4.2) or IL/PF ($n = 7$ optic fiber in $n = 2$ mice, AP:-1.9 or 2.3 mm; ML: -0.8 mm; DV: -2.5 or -2.8 mm). Mice recovered from surgery and the viruses could transfect the PRF/GlyT2+ cells for 3 weeks before behavioral testing or juxtacellular recording. The optic fibers were labeled with Dil stain (1,1'-Diocadecyl-3,3',3'-Tetramethylindocarbocyanine Perchlorate ('Dil'; DilC18(3); ThermoFisher Scientific, #D282).

For further investigation of the PRF/GlyT2+-thalamic pathways, we labeled the axon arbors of PF targeting PRF/GlyT2+ cells ($n = 3$ in GlyT2-Cre mice). We injected AAvg-EF1a-DIO-FloP-WPRE-HGHPa (RRID:Addgene_87306) virus into the Pf unilaterally (AP: -2, ML: 0.5, DV: 3; 30 nL). After three weeks we injected AAV2/1-EF1a-fDIO-EYFP (RRID:Addgene_55641) or AAV2/1-Ef1a-fDIO mCherry (RRID:Addgene_114471) into PRF unilaterally (AP:-4.4, ML:0.8, DV: 4.2, 100 nL).

For examining PRF/vGluT2+ and PRF/vGAT+ projections in the Gi we used vGAT/t2A-FloP//BAC-vglut2/cre mice ($n = 3$). We injected mixed AAV5-hSyn-DIO-mCherry (RRID:Addgene_50459) and AAVDJ-EF1a-fDIO-EYFP-WPRE viruses (based on Addgene plasmid RRID:Addgene_55641, UNC Vector Core) into the PRF unilaterally (AP:-4.4, ML:0.8, DV: 4.2, 100 nL; 1:1 ratio of the viruses).

Histology

Perfusion and tissue fixation

Perfusions were performed under deep anesthesia (sodium pentobarbital 60 mg/kg). Using saline and a fixative solution (0.1% glutaraldehyde (wt/vol) (Electron Microscopy Sciences, #16210) and 4% paraformaldehyde (wt/vol) (TAAB Laboratory, #P001) in 0.1 PB. A peristaltic pump perfused the solutions through the ascending aorta. After the fixation, the brain was sectioned using a vibratome (50 μ m coronal slices).

Immunohistochemistry

For all immunostaining methods, we used TBS buffer. The sections were incubated in sucrose solutions for cryoprotection and were frozen above liquid nitrogen to help the penetration of the antibodies, followed by BSA treatment (4% 40 min). To visualize the L5 fibers (ChR2-mCherry viral tracer) we used a rabbit anti-mCherry polyclonal primary antibody, unconjugated (1:4000 or 1:1000,

(BioVision Cat# 5993-100, RRID:AB_1975001, overnight). To label GlyT2+ cells and fibers in the PRF and in the IL/Pf (in the case of eYFP containing viral tracers or in the Rbp4/cre//BAC_glyt2/GFP mouse line), the sections were treated with chicken anti-eGFP polyclonal primary antibody (1:15000 or 1:1000, (Thermo Fisher Scientific Cat# A10262, RRID:AB_2534023)).

For light and electron microscopic analysis when we visualized the L5 fibers in the brainstem after the anti-mCherry primary antibody we used.

ImmPRESS-AP Anti-Rabbit Ig Reagent(1:2, (Vector Laboratories Cat# MP-5401, RRID:AB_2336536)) and DAB-Ni/DAB (DAB-Ni: Nickel-intensified 3,3'-diaminobenzidine (bluish-black reaction product), DAB: 3,3'-diaminobenzidine, Sigma-Aldrich, Cat# D5637, brown reaction product) as a chromogen. In the other case, after the anti-eGFP primary antibody (1:15000) we used ABC (avidin biotinylated horseradish peroxidase complex, 1:300, Vector Laboratories, Cat# PK-4000) and DAB as a chromogen.

For fluorescent and confocal microscopic investigations of L5 fibers, after the anti-mCherry primary antibody, we used Cy3-conjugated goat anti-rabbit secondary antibody (1:500, (Jackson ImmunoResearch Labs Cat# 111-167-003, RRID:AB_2313593)) or Cy3-conjugated donkey anti-rabbit (1:500, (Jackson ImmunoResearch Labs Cat# 711-165-152, RRID:AB_2307443)). In the case of the anti-eGFP primary antibody, we used the goat anti-chicken-Alexa488 secondary antibody (1:500, (Thermo Fisher Scientific Cat# A-11039, RRID:AB_2534096)) or Alexa 488 donkey anti-chicken secondary antibody (1:500, (Jackson ImmunoResearch Labs Cat# 703-545-155, RRID:AB_2340375)) to investigate GlyT2//eGFP components.

After juxtaglomerular recordings neurobiotin was visualized with Cy3-conjugated streptavidin (1:2000, Jackson ImmunoResearch Labs Cat# 016-160-084, RRID:AB_2337244)) in the PRF or in the IL/Pf. The GlyT2+ neurons/fibers and the cortical axons were visualized using the same histology mentioned above so we developed DAB-Ni/DAB or fluorescent immunostaining respectively.

To localize the fiber optics and juxtaglomerularly labeled cells, check virus injections, and analyze the fibers in the PRF, all micrographs were taken with OLYMPUS BX61, FLUOVIEW FV1000 confocal microscopy (software: Olympus Fluoview 1.6) or with ZEISS Axio-Plan2 fluorescent microscopy with OLYMPUS DP70 camera (software: Olympus DPCController 1.2.1.108) or Zeiss Axio Imager M1 microscope coupled to an AxioCam HrC digital camera.

Fluorescent microscopy

To verify virus expression and optic fiber placement, fluorescent images were captured using a Panoramic Digital Slide Scanner (Zeiss, Plan-Apochromat 10X/NA 0.45, xy: 0.65 $\mu\text{m}/\text{pixel}$, Panoramic MIDI II; 3DHISTECH, Budapest, Hungary). Every sixth section was stained and analyzed for each animal. Axonal projections in the Gi originating from different cell populations in the PRF were quantified by delineating regions of interest (ROIs) in the Gi (ipsilateral and contralateral, each 0.25 mm^2) based on neuroanatomical landmarks identified using Hoechst counterstaining on fluorescent images, which were delineated with SlideViewer software (3DHISTECH).

Confocal microscopy

Confocal images of the M2/Cg1, IL/Pf, and PRF regions were captured using a Nikon C2 Confocal Laser Scanning Microscope. The imaging was performed with a 4x Plan Fluor objective (NA 0.13, xy resolution 2 $\mu\text{m}/\text{pixel}$), a 10x Plan Fluor objective (NA 0.13, xy resolution 0.63 $\mu\text{m}/\text{pixel}$, z-step size 2 μm), and a 20x CFI Plan Apo VC objective (NA 0.75, xy resolution 0.32 $\mu\text{m}/\text{pixel}$, z-step size 1 μm , Nikon Europe). Confocal microscopy was used to analyze the spatial relationship between M2/Cg1 axonal boutons and labeled dendritic segments in the PRF. eYFP fluorescence was amplified using anti-GFP labeling, and for close apposition analysis, RFP fluorescence was amplified with anti-RFP labeling. To assess close appositions between axonal boutons and dendritic segments in the PRF, high-resolution z stack images (Nikon CFI Plan Apo VC60X/NA 1.40 Oil objective, 0.09 $\mu\text{m}/\text{pixel}$, z-step size 0.3 μm) were taken from 5 μm of the slice. Confocal images were acquired with consistent settings for pinhole size, gain level, axial section depth, and laser intensity across all PRF slices. Close appositions, defined as potential synaptic contacts between labeled axonal boutons and dendritic segments, were manually quantified using NIS Elements Software. The analysis focused on identifying and counting instances where eYFP- or RFP-labeled boutons were in close proximity to EGFP- or RFP-labeled dendritic segments, indicating possible synaptic connections.

Electron microscopy

To analyze the M2/Cg terminals' ultrastructure, we performed immunostaining for the ChR2-mCherry viral tracer (DAB, as described above). To confirm the innervation of PRF/GlyT2+ neurons from M2/Cg, we performed double immunostaining for the ChR2-mCherry viral tracer (DAB-Ni) and GlyT2+//eGFP (DAB) and processed the material for EM. In our hands, the modified DAB-Ni precipitate in the axon terminals could be unambiguously differentiated from the end product of marble-like DAB.

After double immunohistochemistry of L5 terminals and PRF/GlyT2+ cells the sections were treated with OsO₄ (0.5%, vol/vol, with 7% sucrose for 40 min in 0.1 M PBS), followed by dehydration, sequential incubation in ethanol, uranyl acetate, and acetonitrile for ultrastructural analysis. The dehydrated sections were embedded in Durcupan (Sigma Aldrich, Cat# 44610). Blocks containing PRF were re-embedded and sectioned to ultrathin sections (60 nm thick) with an Ultramicrotome (EM UC6, Leica Biosystems). The dendrites and terminals (area, diameter) were measured in three non-consecutive sections in FIJI software.⁵¹

The sections were examined using a HITACHI 7100 electron microscope; the electron micrographs were taken with a Megaview digital camera.

In vitro electrophysiology

The *in vitro* electrophysiological experiments of Figure 2 were performed on coronal slices from the brains of PRF of adult mice (more than 3 months old), see the virus injection method in the previous paragraph.

Slices were prepared for a minimum of 4 weeks following surgery. Briefly, mice were anesthetized with an intraperitoneal injection of pentobarbital, then perfused through the ascending aorta with cold (2°C–5°C) bicarbonate-buffered saline (BBS) containing (in mM): 115 NaCl, 2.5 KCl, 1.6 CaCl₂, 1.5 MgCl₂, 1.25 NaH₂PO₄, 26 NaHCO₃ and 30 glucose. Mice were then decapitated, and the portion of the brain containing the PRF was extracted and placed in BBS at 2°C–5°C for a few minutes. Slices (300 µm) were then cut with a ceramic blade on a 7000smz-2 vibratome (Campden). The slicing procedure was performed in an ice-cold solution containing (in mM): 130 potassium gluconate, 15 KCl, 0.05 EGTA, 20 HEPES, 25 glucose, 1 CaCl₂ and 6 MgCl₂ supplemented with D-APV (50 µM). Slices were then transferred for a few minutes to a solution containing (in mM): 225 d-mannitol, 2.5 KCl, 1.25 NaH₂PO₄, 25 NaHCO₃, 25 glucose, 1 CaCl₂ and 6 MgCl₂, and finally stored for the rest of the experimental day at 32°–34°C in oxygenated BBS (pH 7.4 after equilibration with 95% O₂ and 5% CO₂). For all recordings, slices were continuously superfused at 32°–34°C with oxygenated BBS.

We recorded GFP-positive neurons from PRF.²² PRF identification was facilitated by the presence of the red fluorescent plexus originating from the cortical viral injections, observed via a 530 nm green LED (Thorlabs). Cells were visualized with a combination of infrared Dodt contrast and an on-line video contrast enhancement, using a CoolSnap HQ2 CCD camera (Photometrics) run by MetaMorph (Universal Imaging). Fluorescent glycinergic neurons were identified using a 470 nm-wavelength blue LED (Thorlabs). Both 470 nm and 530 nm LEDs were coupled to the slice chamber via the epifluorescence pathway of the microscope.

Whole-cell, voltage-clamp recordings were performed with an EPC-10 double amplifier (Heka Elektronik) run by PatchMaster software (Heka). Patch pipettes (resistance 2–3 MΩ) were filled with an intracellular solution containing (mM): 110 CsMeSO₃ (Sigma Aldrich, Cat# C1426), 4.6 MgCl₂, 10 HEPES, 10 K₂-creatine phosphate (Calbiochem, Sigma-Aldrich Cat# 237911), 10 TEA-Cl (Sigma Aldrich, Cat# T2265), 0.05 4-AP (Sigma Aldrich, Cat# A1910), 4 Na₂-ATP, 0.4 Na₂-GTP, 1 QX-314 (Tocris), pH 7.35 with CsOH (~300 mOsm). Series resistance was partially compensated (max 65%), whereas liquid junction potentials were not corrected. Stimulation train recordings were performed at a holding potential of –60 mV. The AMPA and NMDA components of the EPSCs were examined at both –60 mV, and +50 mV. The brief (2–3 ms long) flashes of blue light used to evoke synaptic responses were provided by triggering the 470 nm LED. TEA-Cl (500 µM) and 4-AP (50 µM) were added to the perfusing BBS when the AMPA and NMDA components were investigated. This procedure was necessary both for increasing synaptic release probability, and for reducing the sizable current leaks developing at +50 mV in control recording conditions, thus decisively improving EPSC detection.

In vivo electrophysiology

Cortical activation and LFP recording

For *in vivo* investigation of the L5-PRF pathway we activated the M2/Cg L5 cells optogenetically (see above the surgery details in Surgeriess $n = 7$) and electrically (in BAC_Glyt2/GFP mice, $n = 3$). The laser beam was generated by a 473 nm laser (Thorlabs lasers). The laser pulses were 5 ms long, 10 mW intensity, and were delivered at 1,10 and 20 Hz frequencies ($n = 50$ stimulus in 5 trains). When we applied electrical stimulation (1–2 µA) we used a bipolar stimulating electrode on the surface of the cortex (M2/Cg, same position described above).

To record cortical field potentials, bipolar LFP electrodes (FHC, resistance ~1 MΩ) were inserted into the frontal cortex of mice (bregma 1.7 mm; lateral –0.8 mm). The recorded signal was amplified, band-pass filtered from 0.16 Hz to 5 kHz for LFP recordings and from 100 Hz to 5 kHz to record the multiunit activity (Supertech BioAmp, Supertech, Pécs, Hungary) and digitized at 20 kHz (micro 1401 MkII, CED, Cambridge, UK).

Juxtacellular recording

PRF and IL/Pf single unit activity was recorded via glass microelectrodes (*in vivo* impedance of 20–40 MΩ) made from borosilicate glass capillaries (1.5 mm outer diameter, 0.75 or 0.86 inner diameters, Sutter Instrument Co., Novato, CA, USA or WPI Inc. Sarasota, FL, USA). Electrodes were positioned into the PRF (bregma –4.4 mm; lateral –0.8 to –1 mm; ventral from cortical surface –3.8 to –4.8 mm) or IL/Pf (bregma –1.9 to 2.3 mm; lateral –0.8 mm; ventral from cortical surface –2.5 to –2.8 mm) (using a piezoelectric microdrive (Burleigh 6000 ULN or ISS 8200, EXFO, Quebec City, Quebec, Canada). Neuronal signals were amplified by a DC amplifier (Axoclamp 2B, Axon Instruments/Molecular Devices, Sunnyvale, CA, USA), further amplified, and filtered between 0.16 Hz and 5 kHz by a signal conditioner (LinearAmp, Supertech) and recorded by Spike2 5.0 (CED). The electrodes were filled with 0.5 M K⁺ - acetate and 2% neurobiotin (Vector Laboratories, Burlingame, CA, USA, #SP-1120). Juxtacellular labeling of the recorded neurons was done by filling the neurons with neurobiotin, as described in.³¹ After the experiments, the animal was perfused, and coronal sections were cut from the whole brain (3.1. Perfusion and tissue fixation). To visualize neurons filled with neurobiotin and to determine their GlyT2 content (in the PRF) or whether it is surrounded by PRF/GlyT2+ fibers (in IL/Pf), we treated the sections as described in 3.2. Immunohistochemistry. The GlyT2eGFP positivity was determined by confocal microscopy.

Cortical spreading depression

The local application of 1M potassium chloride (KCl) or tetrodotoxin (sodium channel inhibitor) induced CSD.³² The onset of cortical activity suppression happened after a few minutes and lasted for 15–20 min. To facilitate the normalization of cortical activity the cortical surface was rinsed with saline several times.

Janelia mouse light Neuron Browser

We analyzed single-cell reconstruction data of the Mouse Light Neuron Browser (<https://www.janelia.org/open-science/mouselight-neuronbrowser>)³³ by identifying PRF-projecting M2/Cg L5 neurons, we selected neurons that have their soma in M2 or Cg area and projected to the PRF. In the browser, we could set the threshold to the axonal projection, called the in the browser “axonal endpoint”.

We used 4 thresholds: ≥ 10 , 5–10, 2–5, or 1. We always precisely checked the anatomical region to uniform terminology that we used during our research (Paxinos atlas vs. Neuron Browser).

Behavior

Experimental protocol

After virus injection and optic fiber implantation (see above) the experimental protocol included handling (2 weeks), habituation (3 days), and the optogenetic experiment. The handling period started 1 week after the surgery. During the habituation, we placed the mouse in the experimental box and connected their optic fiber to a fiber optic patchcord (Thorlabs) and the patchcord cable (Thorlabs). The mice moved freely in the experimental box and got used to the new environment and the weight of the cable and the mouse was allowed to move passively. During the experiment phase, we photoactivated or inhibited the transfected PRF/GlyT2+ cells or their fibers in IL/Pf. The photoactivation was generated by a 473 nm DPSS laser (LRS-0473-PFM-00050-03, Laser-glow Technologies, Toronto, Canada). The photoinhibition was generated by 589 nm DPSS laser (LRS-0589-GFF-00100-05, Laser-glow Technologies, Toronto, Canada). The photostimulation trains were 10 s long, 5 ms light pulses at 40 Hz in PRF every 1 min in 4 laser intensities (1, 5, 10, 15 mW). The photoinhibition trains were 10s long, and continuous stimulation. We stimulated every condition (every optic fiber) 20 times (5-5-5-5 stimulation by intensities), and the experiment took about 30 min. During IL/Pf stimulation we used 30 Hz. After the experiments, we perfused the animals and identified the location of the virus injection and the optic fibers post hoc (see Histology).

QUANTIFICATION AND STATISTICAL ANALYSIS

Axonal density analysis

For intensity density analysis, FIJI was used to split the color channels of each image into red, green, and blue. The relevant channel (red for RFP, green for eGFP) was converted to grayscale. Background noise was removed, and the 8-bit images were then converted to binary with a consistent threshold for the reporter protein (RFP or eGFP). This allowed for precise calculation of axonal density within the selected regions. Axonal density in each image was calculated and expressed as the mean area percentage. To compare the ipsilateral and contralateral axonal densities statistically, the data were normalized to the ipsilateral side.

Density mapping analysis

Following fluorescent immunostaining, we investigated the density of L5 fibers in the PRF. A map based on fiber density was created by FIJI software1662. A high-magnification confocal micrograph was taken about PRF/GlyT2+ cells and M2/Cg L5 fibers (20x, NA: 0.75). The pictures were converted to 8-bit in depth then the brightest pixels of single optical slices of the original image stacks were projected into one plane to depict all of the labeled bright structures. These maximum intensity projections were smoothed by a Gauss filter with a radius of 40 pixels then the pixels were ordered according to their intensity values in 8 categories. The result is a pseudocolored, semi-quantitative map of the fiber density that enables the localization of the highest fiber density areas in a given image.

In vitro analysis

Sampling frequency was 40 kHz. Data was filtered at 3 kHz. All data were analyzed using routines developed in-house with Igor (Wavemetrics). Statistical comparisons were performed using either the Mann-Whitney test for unpaired values, or the Wilcoxon Signed-Rank test for paired sets of data, as indicated in the text. Statistical significance was set at 0.05. Results are given as mean \pm s.e.m.

Analysis for juxtacellular recordings

All statistical analysis was performed in R Statistical Computing Software (R Core Team (2021). (R: A language and environment for statistical computing. R Foundation for Statistical Computing, Vienna, Austria. URL <https://www.R-project.org/>).

PFC photoactivation

To evaluate the effect of photoactivation the first APs following each stimulus were detected in a 40 ms window. They were distributed around ~ 10 ms peak with variable spread. Only APs in the [25th percentile - 1.5*IQR, 75th percentile + 1.5*IQR] & AP time >0 ms range were considered evoked response. APs occurring outside of this range were considered baseline firing activity and were excluded from further analysis.

Response probabilities were calculated as the number of evoked APs/number of stimuli*100 and plotted alongside the median latency values.

Spontaneous frontal cortical activity changes

To determine synchronous and desynchronous periods the raw LFP signal was filtered, down-sampled, and standardized. The power spectral density of each LFP signal was calculated, and the dominant frequency was determined. To find the synchronous and desynchronous periods of the cortical LFP signal, the standard deviation of the signal amplitude was calculated in overlapping sliding

windows. The size of the sliding window was equal to the length of one cycle, and the overlap was half a cycle. The threshold for synchronous and desynchronous periods was placed halfway between the median and the 25th percentile.

The number of clusters was calculated in the synchronous and desynchronous periods and was statistically compared using the Wilcoxon test. Action potential clusters were determined by separating the two peaks at the minimum bimodal inter-spike interval histograms (ISI). The number of bins of the ISI was determined by the Freedman-Diaconis rule for optimal bin width; the window size was equal to the length of one cycle of the slow cortical oscillation. The mean cluster rate per LFP state was calculated by dividing the number of clusters by the length of the corresponding LFP states in every recording.

The mean firing rate (MFR) was calculated by dividing the sum number of action potentials divided by the sum lengths of the corresponding LFP states in every recording.

Thalamocortical neuronal activity

MFR before, during, and after stimuli were calculated as the sum number of APs divided by the sum length of each epoch. Based on the efficacy of the photo-stimulation the cells were divided into *weak* and *strong inhibition* categories. If the ratio of the number of APs +1s after and -1s before the stimulus was larger than 0.75 (number of spikes only dropped a little shortly after stimulus onset) the cell was categorized as weakly inhibited, if it was smaller than 0.75 (big drop of spike numbers shortly after stimulus onset) the cell was categorized as strongly inhibited.

Video analysis for behavior

To analyze the movements during the experiment we used Simple Mouse Tracker (SMT) downloaded from GitHub. SMT is a video tracker software based on Open CV that runs on any platform that supports Python. It is designed to track the body, head, and tail coordinates (X, Y) of a single-colour mouse over a homogeneous color background. <https://github.com/joseaccruz/SimpleMouseTracker>.

After cleaning the tracking data (removing noise, outliers, and missing data) the before-stimulus speed and rotation of the animals were compared with the during-stimulus and -in the rotation experiments-to the after-stimulus periods.

To get the speed of the animals the Euclidean distance of the center (body) points across every 5th frame was calculated and converted to mm (scaling factor: 1.6 mm/pixel). To get the rotation of the animal the signed angle of the body-head vector was calculated across every frame and the mean rotation angles across frames were plotted.

For traveled distance plots every 5th frame (data point) was used (25 fps, scale: 1.6 pixel/mm). We calculated distances and average speed (mm/s) across every 5th frame. Traveled distance (mm/s) is averaged through the last second of the “before stimulus” category and the first second of the stimulus and the last 9 s of the stimulus. Traveled distance “after stimulus” is not included.

For rotation, we plotted every frame (data point). To show the animal’s movement trajectory during stimuli the head-center-tail body points were plotted, separately in non-stimulated and stimulated periods. We calculated vectors (based on head-body X-Y co-ordination) and measured the mean angle changes of every vector. After that, we multiplied that number with fps values and divided that number by 360 to get which is the mean rotation angle during 1 s relative to one whole circle. That value was multiplied by 100 to obtain the percentage of rotation within 1 s in relation to a complete circle. The global angle threshold used in this file is 90. Grater rotation angles between consecutive frames are replaced by zero.

Statistics

In all behavioral and electrophysiological experiments, mice were randomly assigned to groups. Data points from animals with misplaced viral infections were excluded from analysis. The number of animals used in each experiment is specified in the respective figure legends. All data were checked for normality, and outliers were defined as values outside the range of Q1 - 3IQR and Q3 + 3IQR. All statistical analyses were performed using R Statistical Environment, Jamovi v 2.328, and Prism 8 software (GraphPad Software). For the juxtacellular analysis, the following statistical methods were applied: Mood’s median test (two-sided), Wilcoxon Signed-Rank Test (one-sided and two-sided, depending on the measure), and the Mann-Whitney test (two-sided). *In vitro* analysis utilized the Wilcoxon Signed-Rank Test. Behavioral data were analyzed using Friedman ANOVA with the Durbin-Conover post-hoc test, Wilcoxon Signed-Rank Test (one-sided), and the Mann-Whitney test (two-sided). Ipsilateral and contralateral axonal projection density was analyzed using a two-sided paired t test.

The asterisks define the levels of statistical significance in hypothesis testing: * 0.05 < p; ** 0.01 < p; ***p < 0.001; n.s. - no significant difference.